CHAPTER 3

Mechanism of life-long maintenance of neuron identity despite molecular fluctuations

Joleen J. H. Traets[1], Servaas N. van der Burght[2], Gert Jansen[2], Jeroen S. van Zon[1]

[1]AMOLF, Amsterdam, the Netherlands.
[2]Dept. of Cell Biology, Erasmus University Medical Centre, Rotterdam, the Netherlands

Submitted for publication

ABSTRACT

Cell fate is maintained over long timescales, yet molecular fluctuations can lead to spontaneous loss of this differentiated state. We uncovered a mechanism that explains life-long maintenance of ASE neuron fate in *C. elegans* by the terminal selector transcription factor CHE-1. Fluctuations in CHE-1 level are buffered by the reservoir of CHE-1 bound at its target promoters, which also ensure continued *che-1* expression by preferentially binding to the *che-1* promoter. We validated this mechanism by showing that *che-1* expression was resilient to induced transient CHE-1 depletion, while both expression of CHE-1 targets and ASE function were lost. We identified a 130 bp-long *che-1* promoter fragment responsible for this resilience, with deletion of a homeodomain binding site in this fragment causing stochastic loss of ASE identity long after its determination. Because network architectures that support this mechanism are highly conserved in cell differentiation, such mechanism may explain stable cell fate maintenance in many systems.

INTRODUCTION

In most animal tissues, terminally differentiated cells are renewed from progenitor cells on timescales of days to months (Leblond and Walker, 1956), yet the nervous system is unique, as most neurons hardly renew at all (Ming and Song, 2005). Many mature neuron subtypes exist that differ in the expression of hundreds of subtype-specific genes (Deneris and Hobert, 2014). How neuronal cells maintain this terminally differentiated state over such long timescales—decades in the case of humans—is not understood.

Recent studies have found that differentiation preceding maturation of neuron subtypes is often controlled by only 1 or 2 different transcription factors, called *terminal selectors* (Hobert, 2016). These act through a conserved network motif called a single-input module (Alon, 2007): they bind to specific *cis*-regulatory control elements to induce both their own expression and that of the downstream target genes that define the neuronal subtype (Fig. 1A). Such terminal selector networks have been found to underlie differentiation of many neuron types in the nematode *Caenorhabditis elegans* (Deneris and Hobert, 2014; Hobert, 2016), photoreceptor subtypes in *Drosophila melanogaster* (Hsiao et al., 2013) and dopaminergic neurons in mice (Ninkovic et al., 2010), indicating that they form an evolutionary conserved principle for neuron subtype determination.

Terminal selectors positively regulate their own expression, raising the possibility that they act as bistable genetic switches. Such switches are wide-spread in biology (Ferrell, 2002; Alon, 2007) and are often seen as an attractive mechanism to explain cell fate determination. In this hypothesis, at the time of determination, transient signals induce expression of terminal selectors, which then maintain their own expression, and that of all target genes, by autoregulation in the subsequent absence of these signals (Fig. 1B) (Hobert, 2008). However, a key weakness of bistable switches is that they remain reversible at all times, with a transient decrease in terminal selector levels potentially sufficient to lose terminal selector expression and, presumably, cell fate (Fig. 1B). Indeed, bistable genetic switches often suffer from stochastic transitions between their different states due to molecular noise, i.e. random fluctuations in the levels of their core components (Ozbudak et al., 2004; Suel et al., 2006; Acar et al., 2005). Hence, it is often assumed that stable cell fate maintenance must require additional feedback mechanisms, such as histone or chromatin modifications (Orlando, 2003; Ringrose and Paro, 2007), that lock-in cell fate in an essentially irreversible manner.

Here, we studied long-term maintenance of neuron subtype in the salt-sensing ASE neurons of *C. elegans* (Fig. 1A). ASE subtype is controlled by the terminal selector CHE-1, a transcription factor whose mRNA expression is transiently induced by the nuclear hormone receptor NHR-67 at the time of determination (Sarin et al., 2009). CHE-1 induces the expression of 500-1000 ASE target genes, such as genes encoding chemosensory receptors, ion-channels, and neuropeptides, by binding ASE motifs within their promoters (Etchberger et al., 2007).

Continued presence of CHE-1 is required for expression of target genes after neuron subtype determination (Etchberger et al., 2009). CHE-1 also upregulates its own mRNA expression. This positive feedback loop is necessary for sustaining *che-1* expression and ASE cell fate directly after cell determination (Etchberger et al., 2007; Leyva-Diaz and Hobert 2019). Yet, it is unknown whether this positive feedback loop is sufficient for long-term maintenance of ASE fate. The impact of molecular noise, such as variability in CHE-1 protein number, on ASE fate maintenance has not been studied. Overall, it is an open question whether a reversible, bistable switch based on positive CHE-1 autoregulation would be sufficiently stable to maintain ASE fate during the animal's entire lifetime. Alternatively, additional mechanisms could be necessary to ensure that, once ASE fate is determined, *che-1* expression becomes independent of CHE-1 itself and can no longer spontaneously switch off.

We show that sufficiently long, transiently induced depletion of CHE-1 caused permanent loss of ASE fate, indicating that it is controlled by a switch that remains reversible long after cell fate commitment. This raises the question how the switch is protected against molecular noise, which could cause it to spontaneously lose ASE fate. Combining experimental measurements of the key parameters that control the magnitude of noise, i.e. the *che-1* mRNA and protein numbers and lifetimes, with stochastic models of the *che-1* genetic network, revealed a novel mechanism, *target reservoir buffering*, that dramatically increased switch stability. This stability resulted from the presence of a reservoir of CHE-1 protein bound at the promoters of its target genes, coupled with preferential binding of CHE-1 to the *che-1* promoter compared to the promoters of its other targets. Our model suggests that this mechanism leads to exceedingly stable ON states (high *che-1* expression), with spontaneous transitions to the OFF state (no *che-1* expression) observed at rates of less than 0.001 per year. Consistent with this mechanism, we found that upon induced CHE-1 depletion *in vivo*, *che-1* mRNA expression remained present, even when expression of other target genes vanished together with the animal's ability to respond to salt. This allowed full recovery of CHE-1 protein levels, target gene expression and chemosensation if induced CHE-1 depletion was sufficiently short. We found a 130 bp-long promoter region surrounding the *che-1* ASE binding motif responsible for this resilience of *che-1* expression to CHE-1 depletion. This region contained a homeodomain protein binding site that, when mutated, caused stochastic loss of ASE fate well after ASE specification, indicating a strong decrease in stability of the ON state. This shows a new role for homeodomain containing transcription factors in maintaining and stabilizing ASE fate, likely by recruiting CHE-1 preferentially to its own promoter.

RESULTS

Loss of ASE neuron fate upon transient CHE-1 depletion

To test whether positive autoregulation of *che-1* expression is necessary for ASE fate maintenance, we depleted CHE-1 protein levels in ASE neurons in vivo, using the auxin inducible degradation system (Zhang et al., 2015). *che-1::GFP::AID* animals were exposed to 1 mM auxin to induce CHE-1 depletion (Fig. 1C). CHE-1::GFP was strongly reduced after ~1.5 hour, and undetectable after ~4 hours exposure to auxin (Fig. 1D). To examine how CHE-1 depletion impacted on ASE function, we used a quadrant chemotaxis assay to quantify the chemotaxis response to NaCl of CHE-1 depleted animals (Wicks et al., 2000; Jansen et al., 2002). In this assay, animals choose between two agar quadrants with salt and two without (Fig. S1A). *che-1::GFP::AID* animals exposed to auxin for 24 hours showed reduced chemotaxis to NaCl ($P<0.001$) (Fig. 1E, S1C). This agrees with previous results showing that permanent inhibition of *che-1* expression by RNAi in larvae resulted in reduced expression of CHE-1 target genes (Etchberger et al., 2009). However, these results leave open the possibility that, after initial ASE subtype determination, *che-1* expression is maintained independently of CHE-1 in an irreversible manner.

In contrast, if *che-1* expression is bistable and reversible, then a sufficiently long period of transient CHE-1 depletion should result in permanent loss of *che-1* expression (Fig. 1B). To test this, we exposed animals to auxin for increasing time intervals (Fig. 1C), and analysed CHE-1::GFP expression and NaCl chemotaxis after 24 (Fig. 1D, S1B,C) or 48 hours (Fig. 1E,F) recovery on plates without auxin. In animals exposed to auxin for 24 hours, both CHE-1::GFP expression and NaCl chemotaxis returned to wild-type levels after 24 hours recovery. However, after 48 hours auxin exposure, CHE-1::GFP did not return in 11/41 animals (Fig. 1F, S1B). This fraction further decreased with the duration of auxin exposure, with 0/9 animals recovering CHE-1::GFP expression after 120 hours on auxin. Similarly, the chemotaxis response did not recover in animals exposed to auxin for 96 hours or longer (Fig. 1E, S1C; Table S1), suggesting that the absence of CHE-1::GFP resulted in loss of ASE subtype identity. Overall, these observations indicated that CHE-1 controls its expression as a bistable switch that can withstand strong decreases in CHE-1 level for a limited time, but nevertheless remains fully reversible long after its induction.

Number and lifetime of che-1 mRNA and protein

The observed reversibility of the ON state raises the question how spontaneous transitions to the OFF state, due to random fluctuations in CHE-1 level, are prevented under normal conditions. Theoretical studies of genetic switches suggest that the probability of such transitions decreases with increasing the concentration and lifetime of the transcription factors involved (Warren and ten Wolde, 2005; Walczak et al., 2005; Mehta et al., 2008). Therefore, we determined the *che-1* mRNA copy numbers and protein concentration, and their lifetimes.

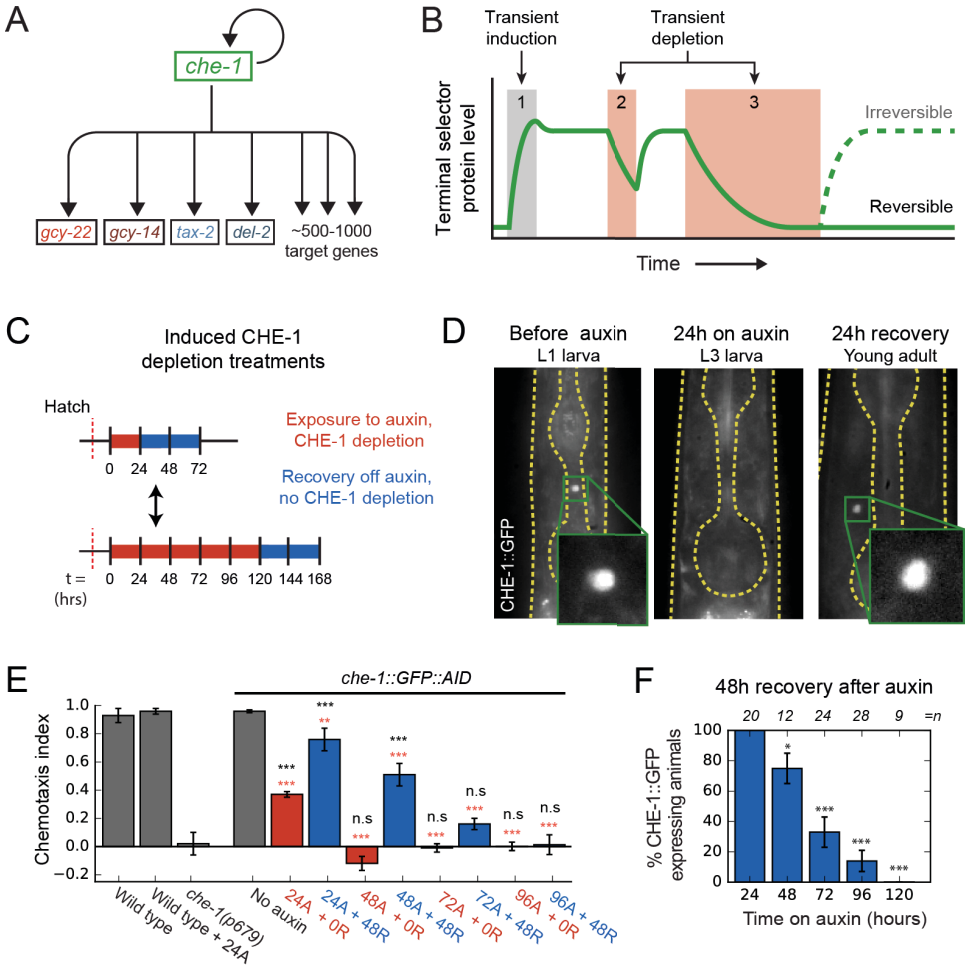

Figure 1. Loss of ASE neuron fate upon transient CHE-1 depletion. (A) The terminal selector gene *che-1* induces its own expression and that of 500-1000 target genes that together determine ASE neuron fate. Positive autoregulation of *che-1* expression could result in bistable, switch-like behaviour. **(B)** Bistability generates sustained terminal selector expression upon transient induction (1), that is resilient to short periods of terminal selector depletion (2). However, bistable switches remain reversible and will lose terminal selector expression upon sufficiently long depletion (3), while irreversible switches will always recover. **(C)** Transient CHE-1 depletion using Auxin-Induced Degradation (AID). *che-1::GFP::AID* L1 larvae (CHE-1::GFP) or young adults (chemotaxis) were exposed for different time periods to 1 mM auxin to induce CHE-1 degradation, and were subsequently characterized after a 24 or 48 hours recovery period. **(D)** CHE-1::GFP fluorescence in *che-1::GFP::AID* animals before (left) and after 24 hours auxin treatment (middle), and after a subsequent 24 hours recovery off auxin (right). Even though CHE-1::GFP is lost from ASE neurons after auxin treatment, it reappears after recovery off auxin. **(E)** Response to 10 mM NaCl for wild-type animals, *che-1(p679)* mutants defective in NaCl chemotaxis, and *che-1::GFP::AID* animals exposed to auxin for 24-96 hours (24A – 96A) tested directly (0R) or after 48 hours recovery (48R). *che-1::GFP::AID* animals on auxin showed a chemotaxis defect similar to *che-1(p679)* mutants. *che-1::GFP::AID* animals recovered chemotaxis to NaCl after 24 or 48 hours on auxin, but exhibited a persistent chemotaxis defect after sufficiently long, transient CHE-1::GFP::AID depletion. **(F)** Fraction of animals that recovered CHE-1::GFP expression 48 hours after auxin treatment of increasing length. No animals recovered CHE-1::GFP expression after 120 hours of CHE-1 depletion. Error bars in E and F represent mean of 4 assays ± S.E.M. *P<0.05, **P<0.01, ***P<0.001, in E significance is compared to che-1(p679) mutants (black) or no auxin (red).

First, we measured the absolute number of *che-1* mRNA and protein molecules in ASE neurons. We used single-molecule FISH (smFISH) (Ji and van Oudenaarden, 2012) to count individual *che-1* mRNA molecules. As a benchmark, we also measured mRNA levels of the putative NaCl receptors *gcy-14* and *gcy-22*, and the ion channel subunits *del-2* and *tax-2,* which are CHE-1 target genes with >1 ASE motif in their promoter region (Ortiz et al., 2009; Coburn and Bargmann, 1996). In embryos, we found that *che-1* mRNA levels peaked at 26±6 mRNAs/cell during the bean stage, i.e. the time of ASE neuron determination (Fig. 2A,B), and fell to 6±3 mRNAs/cell from the comma stage onwards. In contrast, the CHE-1 target gene *gcy-22* showed a steady increase in mRNA levels during development and surpassed *che-1* mRNA expression after the 1.5-fold stage. In larvae, we also found low *che-1* mRNA levels, with 5±2 mRNAs in the left (ASEL) and 7±3 mRNAs in the right ASE neuron (ASER). *che-1* expression was low compared to the panel of CHE-1 target genes examined (Fig. 2C,D), with *del-2*, *gcy-14* and *gcy-22* expressed at significantly higher levels. Moreover, *che-1* mRNA levels remained low during all four larval stages, L1-L4, with slightly higher mRNA levels in the ASER, compared to the ASEL neuron (Fig. 2E). For this entire period, the target genes with the highest expression, *gcy-14* and *gcy-22*, remained expressed well above *che-1* levels. Overall, these results show that *che-1* expression is biphasic: an initiation phase with high *che-1* expression level when ASE fate is induced in the embryo, followed by a maintenance phase with *che-1* expressed at a low level where molecular fluctuations likely have significant impact.

We also estimated the absolute CHE-1 protein concentration in the ASE neurons. We immersed endogenously tagged *che-1::GFP* animals (Leyva-Diaz and Hobert 2019) in eGFP, and calculated the CHE-1 protein number by comparing the CHE-1::GFP fluorescence inside the ASE neurons with the ambient fluorescence of eGFP (Fig. 2F) (Gregor et al., 2007). For all stages of post-embryonic development, we found an average of 900±250 (~325 nM) and 600±120 (~260 nM) CHE-1::GFP molecules/cell for the ASER and ASEL neuron, respectively (Fig. 2F, S2A), with slightly lower numbers observed in the embryo (Fig. S2B). Overall, the observed range of CHE-1::GFP protein levels, 500-1400 molecules/cell, is comparable to the number of CHE-1 binding sites, 500-1000, in the promoters of CHE-1 target genes, as estimated by the number of ASE motifs detected previously (Etchberger et al., 2007) and by our analysis, indicating that CHE-1 targets compete for a limited pool of CHE-1 protein.

Next, we measured *che-1* mRNA and protein lifetimes. To determine *che-1* mRNA lifetimes in ASE neurons, we transiently overexpressed *che-1* mRNA, using a *hsp16.41p::che-1* heat shock inducible construct (Patel and Hobert, 2017). By exposing animals to 37ºC for ~10 min., we raised *che-1* mRNA levels in the ASE neurons 5-fold, to 24±4 mRNAs/cell ~10 min. after heat shock (Fig. 3A,B). Next, we shifted animals to 20ºC to return *che-1* expression to its pre-induction level and fixed animals at ~17 min. intervals to quantify *che-1* mRNA levels using smFISH. We found that *che-1* mRNA levels returned to pre-induction values after ~60 min. By fitting the measured *che-1* mRNA levels to an exponential function, we obtained a *che-1*

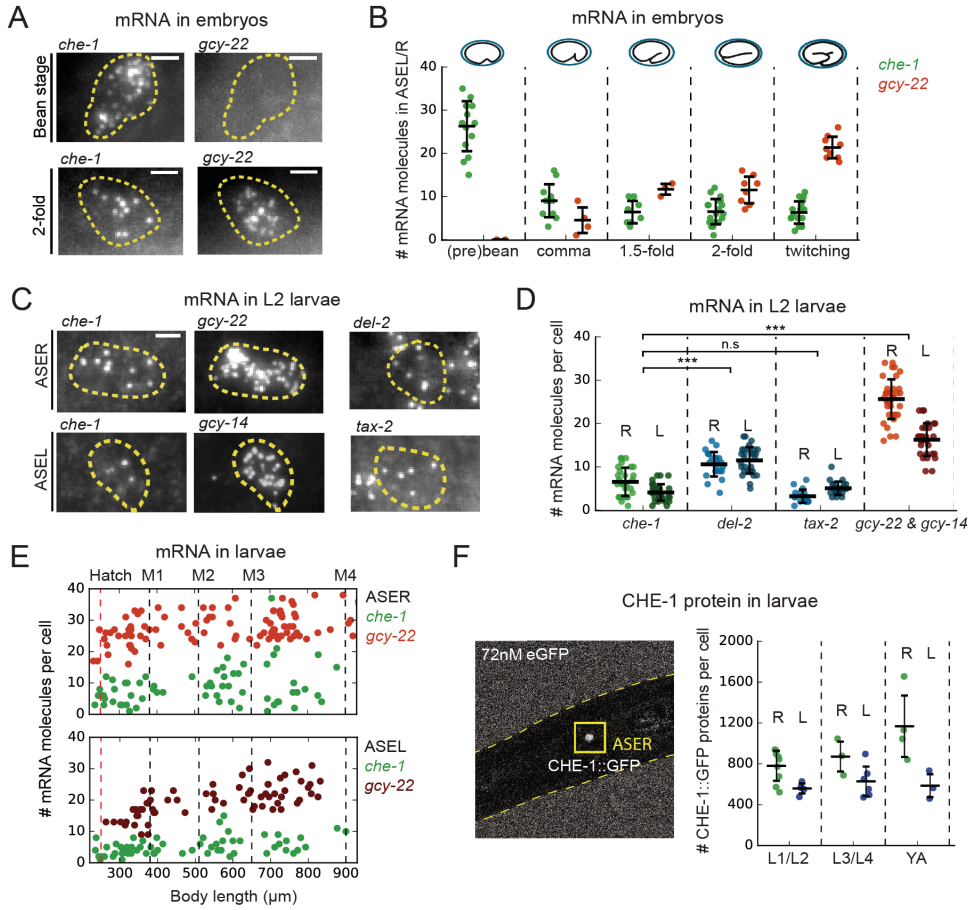

Figure 2. che-1 mRNA and protein copy numbers in ASE neurons. (A) Expression of *che-1* and the CHE-1 target *gcy-22* in embryos at the bean (top) and 2-fold stage (bottom). Each spot is a single mRNA molecule visualized by single molecule FISH (smFISH). Dashed lines outline ASE neuron cell bodies. Scale bar: 2 µm. **(B)** *che-1* (green) and *gcy-22* (red) mRNA levels during embryonic development. *che-1* expression peaks during specification but falls as expression of CHE-1 target genes rise. **(C)** Expression of *che-1* and CHE-1 targets *gcy-22, gcy-14, tax-2* and *del-2* visualized by smFISH in L2 larvae. Dashed lines outline left and right ASE neurons (ASEL/R). Scalebar: 2 µm. **(D)** Quantification of expression of *che-1* and CHE-1 targets in ASEL (L) and ASER (R) in L2 larvae. *che-1* mRNA levels are low compared to other CHE-1 target genes. **(E)** Low *che-1* expression (green, ASER/L) compared to expression of CHE-1 targets *gcy-22* (red, ASER) and *gcy-14* (red, ASEL) throughout larval development. Body length corresponds to developmental time, with approximate timing of hatching and molts between larval stages L1-L4 indicated by vertical lines. **(F)** Left panel: two-photon microscopy image of L2 larva expressing endogenously-tagged CHE-1::GFP, immersed in 72 nM eGFP for calibration. Right panel: CHE-1::GFP protein molecules in ASER (green, R) and ASEL (blue, L) at different stages of post-embryonic development. The number of CHE-1 proteins is comparable to the predicted number of CHE-1 binding sites. Error bars in B, D and F represent mean ± SD. ***P<0.001.

mRNA half-life of 17±4 min. To measure CHE-1 protein lifetime, we used Fluorescence Recovery after Photobleaching (FRAP) in CHE-1::GFP animals. CHE-1::GFP was bleached to approximately ~20% of the original fluorescence level and we measured the recovery of the CHE-1::GFP signal over time, until it reached pre-bleaching levels, which occurred within ~3 hours (Fig. 3C,D). To estimate CHE-1::GFP protein lifetime, we fitted an exponential recovery

curve to the experimental data for each individual animal, resulting in an average measured half-life of 83±20 min.

The *che-1* mRNA and protein half-lives are short compared to reported mRNA half-lives in eukaryotes (Fornasiero et al., 2018; Sharova et al., 2009) and average protein half-lives reported in *C. elegans* young adults (Dhondt et al., 2017; Schwanhausser et al., 2011). Overall, these measured lifetimes show that *che-1* mRNA and protein turnover is rapid compared to the 2-3-week lifespan of *C. elegans* during which ASE identity should be maintained.

Stochastic simulations identify stable cell fate maintenance parameters

The measurements of *che-1* mRNA copy numbers, protein concentration, and their lifetimes allowed us to perform realistic simulations of the CHE-1 switch to estimate its stability against stochastic fluctuations. We constructed stochastic models that included production and decay of *che-1* mRNA and protein molecules, binding of CHE-1 to the promoter of *che-1* and target genes, and target gene expression (Fig. 4A). We examined two bistable models that differed in binding of CHE-1 to its own promoter. In the first model, we assume that CHE-1 binds as a monomer to induce *che-1* expression. This model agrees with the observation that the *che-1* promoter contains only a single ASE motif (Etchberger et al., 2007), but lacks cooperativity

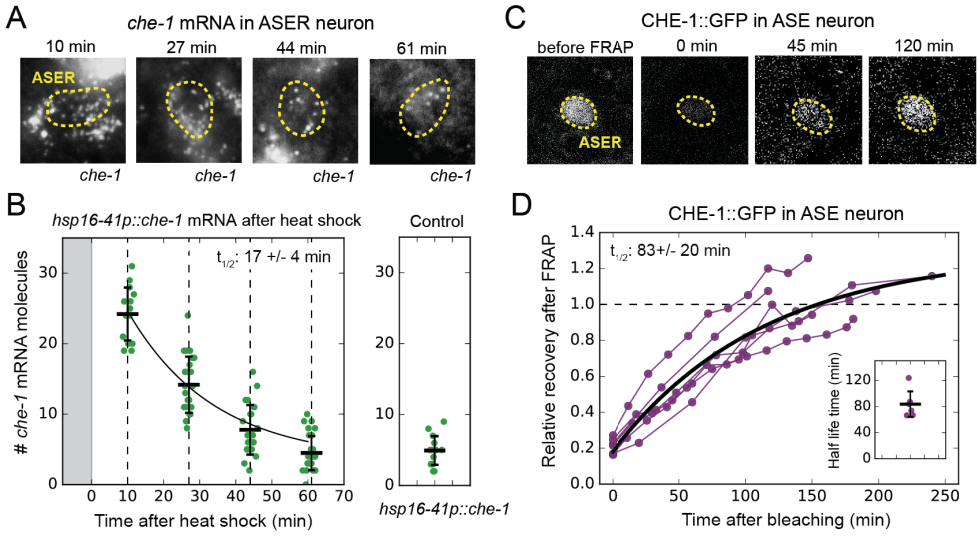

Figure 3. che-1 mRNA and protein lifetimes. (A) *che-1* mRNAs in L2 larvae at different times after induction of *che-1* by a 37°C heat shock in *hsp16-41p::che-1* animals, visualized by smFISH. Dashed lines outline ASER neuron. **(B)** *che-1* mRNA level in ASE neurons of individual L2 animals (green) as function of time after a 10 min. heat shock (grey area). Black line is the fitted decay curve. Control L2 larvae did not receive a heat shock. The measured *che-1* mRNA half-life was 17±4 min. **(C)** CHE-1::GFP fluorescence recovery after photobleaching (FRAP) in the ASER neuron of a single L4 animal. Time is indicated relative to bleaching of CHE-1::GFP. **(D)** Fluorescence recovery of CHE-1::GFP in ASE neurons of L4 or young adult animals (n=6). An exponential recovery curve model was fitted to data of each individual animal (black line indicates the average recovery curve). The inset shows the fitted half-life for each individual animal. The average measured CHE-1::GFP protein half-life was 80±20 min. Error bars in B represent mean ± SD. n≥10 in B and n=6 in D.

in *che-1* induction. Because cooperativity is considered important for generating bistability (Ferrell 2002), we also included a second model wherein *che-1* induction is cooperative, by assuming that expression occurs only when two CHE-1 molecules bind the *che-1* promoter.

The two models have 8 and 9 parameters, respectively, of which experimental data fixed 6 parameters. The production and degradation rates of *che-1* mRNA (f_m,b_m) and protein (f_c,b_c) were fully determined by the measured copy numbers and lifetimes. For the CHE-1 binding rate (f_O) we assumed the diffusion-limited rate, i.e. the highest physically possible binding rate. Based both on previous analysis (Etchberger et al., 2007) and our own, we examined model dynamics for N_T=500 or 1000 CHE-1 target genes, i.e. either smaller or larger than the mean number of CHE-1 proteins (900 molecules/cell). The only free parameters were dissociation rates of CHE-1 from its own promoter (b_0 or b_1,b_2) and from the other targets (b_T). We varied these between 0.1-100 s^{-1}, corresponding to, dissociation constants of ~1-10^3 nM and consistent with values measured for transcription factors (Gebhardt et al., 2013; Jung et al., 2018). We simulated the models using the Gillespie algorithm (Gillespie, 1977). In general, our stochastic simulations showed that molecular noise was sufficiently strong to induce spontaneous transitions from the ON to the OFF state on the timescale of hours or days, indicating that the measured copy numbers and lifetimes by themselves were not sufficient to generate stability against fluctuations. However, we also identified parameter combinations for which the CHE-1 switch remained in the ON state for at least a week (Fig. 4B).

For simulations with high switch stability, brute-force Gillespie simulations were too computationally demanding to directly measure the ON state lifetime. Instead, we used Forward Flux Sampling (FFS), a computational method to efficiently sample rare transition paths between states in multi-stable systems (Allen et al., 2006). Using this approach, we observed parameter combinations with very high stability, i.e. lifetimes of many years, independent of the degree of cooperativity or number of target genes (Fig. 4C, S3A,B). In general, we observed increasing lifetimes for decreasing b_0 or b_1,b_2, i.e. higher occupancy of the *che-1* promoter by CHE-1. Furthermore, the longest lifetimes were found when b_0,$b_2 << b_T$, i.e. when CHE-1 had a much higher affinity for its own promoter than for its other targets. In this regime, we observed average lifetimes of $> 1 \cdot 10^5$ years. Note, however, that despite the long lifetimes in this regime, spontaneous transitions to the OFF state are rapid and occur as a random Poisson process, with a transition possible at any time, albeit with low probability. For such a Poisson process, ON state lifetimes of $> 2 \cdot 10^5$ years are required for the probability of spontaneous loss of ASE fate during their ~2 week lifetime to be less than 10^{-6}, the frequency of spontaneous mutations per gene per generation in *C. elegans* (Anderson, 1995).

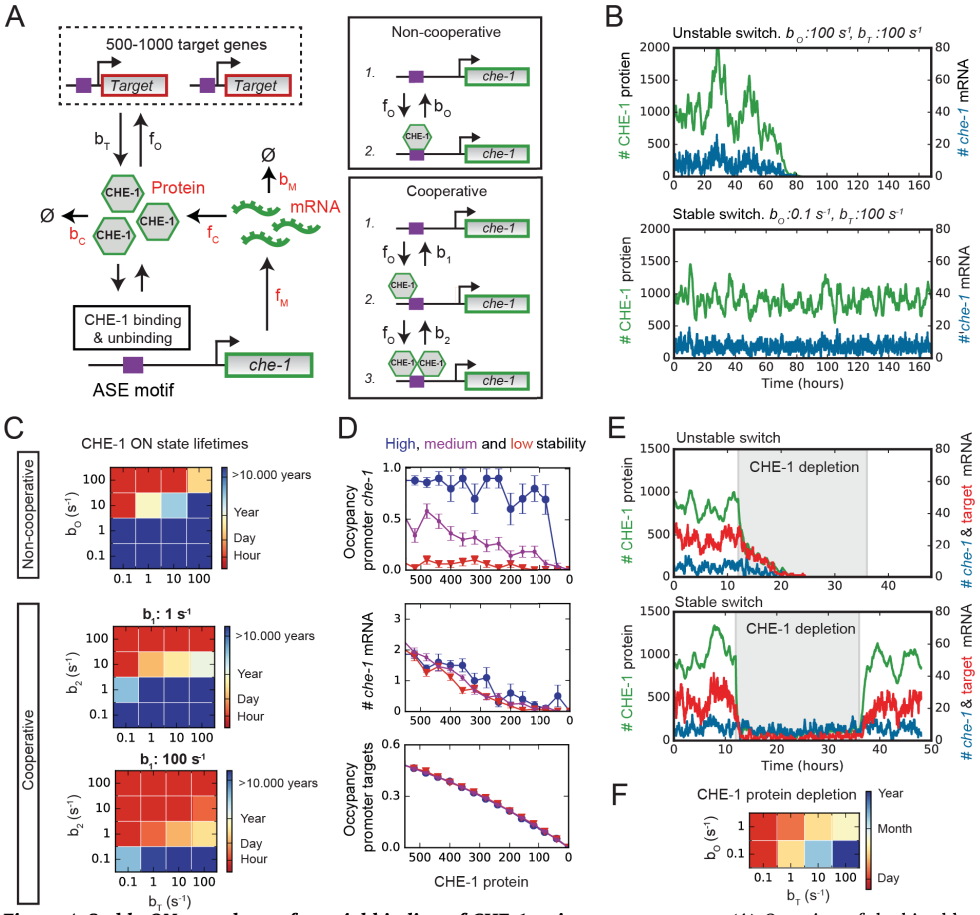

Figure 4. Stable ON state by preferential binding of CHE-1 at its own promoter. **(A)** Overview of the bistable, stochastic CHE-1 switch model, including production and degradation of *che-1* mRNA and protein, and binding of CHE-1 protein to its own promoter and other target genes. Parameters constrained by experimental measurements are red. Inset: CHE-1 binding is modelled either as a monomer (non-cooperative) or as a dimer (cooperative). **(B)** Stochastic Gillespie simulations of the non-cooperative model for parameters with an unstable (top) or stable (bottom) ON state (*che-1* expression), showing levels of *che-1* mRNA (blue) and protein (green). For parameters resulting in an unstable switch, stochastic fluctuations induce a spontaneous transition to the OFF state (no *che-1* expression). **(C)** Average ON state lifetimes calculated using Forward Flux Sampling (FFS) as function of the dissociation rates of CHE-1 from its own promoter (b_O or b_1,b_2) and its target genes (b_T) for the non-cooperative and cooperative model. Long ON state lifetimes occur for high *che-1* promoter occupancy by CHE-1 (b_O<1 or b_1,b_2<1) and preferential affinity of CHE-1 for its own promoter compared to that of its target genes ($b_O << b_T$ or $b_2 << b_T$). **(D)** Average CHE-1 occupancy of the promoter of *che-1* (top) and other target genes (bottom), and average *che-1* mRNA level (middle) during spontaneous transitions from the ON to the OFF state, as sampled by FFS. Shown are transition paths for parameters with low (red, b_O = 100 s^{-1}), medium (magenta, b_O = 10 s^{-1}), and high (blue, b_O = 1 s^{-1}) stability of the ON state, with b_T = 10 s^{-1}. For simulations with a stable ON state, the *che-1* promoter remained fully occupied by CHE-1, even as CHE-1 protein levels approached zero, in contrast to the occupancy of promoters of other CHE-1 target genes. **(E)** Simulations showing the impact of transient depletion of CHE-1 protein (green) on mRNA levels of *che-1* (blue) and a target gene (red). CHE-1 is depleted to 100 molecules/cell by a transient increase in degradation (b_C; grey region). For parameters with an unstable ON state (top), both *che-1* and target gene mRNA levels fall rapidly, and do not recover when CHE-1 depletion ceases. For a stable ON state (bottom), expression of *che-1* is unaffected by CHE-1 depletion, leading to full recovery once CHE-1 depletion ends. **(F)** Average ON state lifetimes, calculated by FFS, during CHE-1 depletion to 100 molecules/cell. Parameter combinations with a stable ON state under normal conditions also maintain *che-1* expression for hours or days under induced CHE-1 depletion.

Stability against stochastic fluctuations by preferential binding of CHE-1 to its own promoter

We found that high stability of the ON state required $b_0,b_2 << b_T$, i.e. CHE-1 binds its own promoter much more strongly than that of its other targets. An explanation for this emerged when we compared transition paths for spontaneous transitions to the OFF state, between parameter combinations that exhibited high (> $1{\cdot}10^5$ years lifetime), medium (~12 days lifetime) and low (~5 hours lifetime) stability (Fig. 4D, S3C). For parameters with low stability we found that, as CHE-1 protein levels fell during spontaneous transitions to the OFF state, both the average *che-1* mRNA number and the fraction of CHE-1 target promoters occupied by CHE-1 decreased, with very low occupancy even of the *che-1* promoter itself close to the end of the transition. In contrast, for parameters with high stability, we found that *che-1* promoter occupancy was high, and the *che-1* promoter remained bound by CHE-1 until the end of the transition, whereas CHE-1 binding was lost earlier on other promoters. These results suggested that high stability arises as a result of a strong preference for CHE-1 protein to bind to the *che-1* promoter, thereby making *che-1* expression insensitive to strong, stochastic decreases in CHE-1 level.

To test this idea, we ran simulations that included a transient depletion of CHE-1, implemented by a temporary increase in the CHE-1 protein degradation rate reducing CHE-1 to 100 molecules/cell (Fig. 4E). We found that simulations with unstable switches, i.e. where $b_0,b_2 > b_T$, were highly sensitive to such depletions, with *che-1* mRNA rapidly falling to such low levels that CHE-1 protein levels and, hence, the ON state, were not recovered when CHE-1 depletion ceased. In contrast, even though the mRNA levels of target genes fell rapidly, simulations with highly stable switches maintained normal *che-1* mRNA levels for many days (Fig. 4F, S3D), allowing the system to successfully recover CHE-1 protein levels and the ON state if CHE-1 depletion was removed sufficiently rapidly.

In vivo CHE-1 depletion decreases target gene, but not che-1 expression.

These simulation results were similar to our experimental observation that CHE-1::GFP levels fully recovered even after 24-48 hours of induced CHE-1 depletion (Fig. 1C-F, S1B,C). To test whether this reflected insensitivity of *che-1* expression to low CHE-1 protein levels (Fig. 4E,F), we used smFISH to compare the impact of auxin-mediated CHE-1::GFP::AID depletion at the mRNA levels of *che-1* and other target genes, focusing on *gcy-22* as the most highly expressed in our panel (Fig. 5A,B). Indeed, *gcy-22* mRNA levels were very low in most che-1::GFP::AID animals after 24 hours on auxin. In striking contrast, *che-1* mRNA levels were close to wild-type. After 24 hours without auxin, *gcy-22* mRNA levels had increased significantly (Fig. 5A,B), consistent with the recovery of CHE-1::GFP levels and chemotaxis to NaCl in these animals (Fig. 1D,E). Overall, these results were in full agreement with our model predictions but raised the question what properties of the *che-1* promoter were responsible for its resilience to CHE-1 depletion.

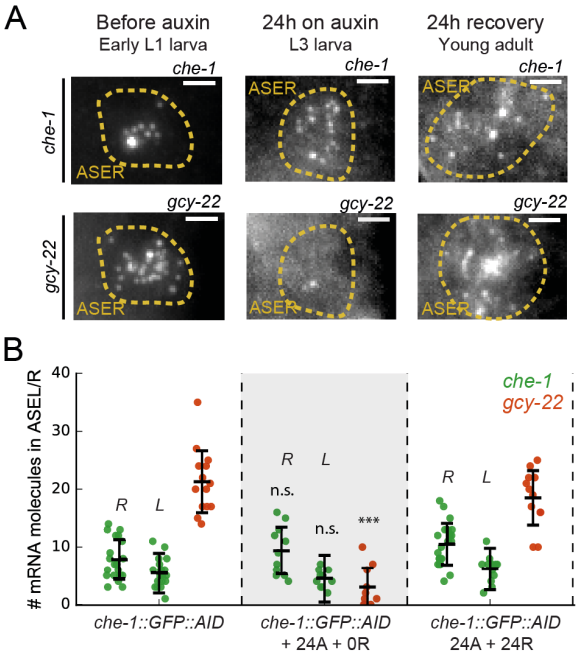

Figure 5. Maintenance of *che-1* expression during transient CHE-1 depletion. (A) *che-1* and *gcy-22* mRNA levels in ASER neurons, visualized by smFISH in *che-1::GFP::AID* animals, at different moments in a 24 hours auxin and 24 hours recovery treatment. Scale bar: 2 µm. **(B)** *che-1* (green, ASEL/R) and *gcy-22* (red, ASER) mRNA levels quantified in *che-1::GFP::AID* animals at different times in a 24 hours auxin and 24 hours recovery treatment. Upon depletion of CHE-1 protein, *che-1* expression was not impacted, while *gcy-22* levels strongly decreased. *gcy-22* expression rose to wild-type levels after 24 hours recovery off auxin. Error bars in B represent mean ± SD. n⩾10. ***P<0.001.

che-1 sequences that flank the ASE motif are required for che-1 expression during CHE-1 depletion

Previous studies identified a single ASE motif 242 bp upstream of the *che-1* ATG start codon as required for autoregulation of *che-1* expression (Etchberger et al., 2007; Leyva-Diaz and Hobert 2019). This ASE motif differs in 6 bp from the sequence in the *gcy-22* promoter, which might explain the divergent effects of CHE-1 depletion on *che-1* and *gcy-22* expression. To test this hypothesis, we used CRISPR/Cas9 in *che-1::GFP::AID* animals to replace the 12 bp ASE motif in the *che-1* promoter with that of *gcy-22*, and vice versa (Fig. 6A). The resulting mutant animals showed wild-type chemotaxis to NaCl and exhibited *che-1* and *gcy-22* mRNA levels similar to wild-type (Fig. 6B,F, S4A), indicating that replacing ASE motifs did not impact ASE specification and target gene expression. Furthermore, when we depleted CHE-1 protein using auxin, *gcy-22* expression in *(ASE_{che-1})p::gcy-22* animals almost completely vanished (Fig. 6F), as in animals with a wild-type *gcy-22* promoter. Overall, the ASE motif itself could not explain the observed differences in *che-1* and *gcy-22* expression. This agrees with previous results that showed a similar calculated affinity score of CHE-1 for the *che-1* and *gcy-22* ASE motif, despite sequence differences (Etchberger et al., 2009).

To examine if promoter regions other than the ASE motif were responsible for the differences in *che-1* and *gcy-22* expression, we replaced ASE motifs together with 59 bp on either side (Fig. 6A). *(ASE_{gcy-22}+flanks)p::che-1* animals exhibited a strong chemotaxis defect and lack of CHE-1::GFP expression in ASE neurons of larvae (Fig. 6B, S4B). At the pre-bean stage, *(ASE_{gcy-22}+flanks)p::che-1* embryos showed high *che-1* expression, 28±7 mRNA/cell, and CHE-1::GFP (Fig. 6C,D, S4B), indicating that *che-1* expression was initiated normally during ASE

determination. However, *che-1* mRNA was absent in *(ASE$_{gcy-22}$+flanks)p::che-1* embryos at later stages. This phenotype was also seen in the *che-1(p679)* loss of function mutant (Fig. S4C) and shows that this 130 bp *che-1* promoter region is important for maintenance of *che-1* expression and ASE fate. *(ASE$_{che-1}$+flanks)p::gcy-22* animals showed wild-type chemotaxis to NaCl (Fig. 6B) and *gcy-22* mRNA levels (Fig. 6F). Yet, strikingly, upon CHE-1::GFP::AID depletion in *(ASE$_{che-1}$+flanks)p::gcy-22* animals *gcy-22* mRNA levels remained high (Fig. 6F), indicating that, like *che-1, gcy-22* expression became resilient to CHE-1 depletion. Hence, the 130 bp *che-1* promoter fragment surrounding the ASE motif is responsible for maintaining expression during CHE-1 depletion.

Involvement of an Otx-related homeodomain binding site in maintaining ASE subtype

Within the 130 bp *che-1* promoter fragment required for resilient *che-1* expression, we identified a high scoring OTX-related homeodomain transcription factor (HD-TF) binding site, 29 bp downstream of the *che-1* ASE motif (Fig. 7A), with only ~60 CHE-1 targets exhibiting a binding site of similar score within 100 bp of their ASE motifs (Table S2, available upon request). To test the function of this HD-TF binding site, we deleted it from the *che-1* promoter in the *che-1::GFP::AID* background. These *(ΔHD)p::che-1* animals showed an intermediate chemotaxis defect (Fig. 7D). To examine whether this defect reflected changes in *che-1* expression we scored CHE-1::GFP expression at different larval stages (Fig. 7B). CHE-1::GFP was expressed in all embryos, but was progressively lost over time, with CHE-1::GFP absent in more than half of the young adults (2/18 animals for ASEL and 9/20 for ASER), indicating a defect in maintenance of *che-1* expression, not in ASE determination. We then used time-lapse microscopy (Gritti et al., 2016) to monitor the dynamics of CHE-1::GFP expression directly in single *(ΔHD)p::che-1* larvae (Fig. S5A). Strikingly, CHE-1::GFP expression was lost in a rapid, stochastic manner (Fig. 7E, S5A), as would be expected for spontaneous, noise-driven transitions to the OFF state. Theoretical studies showed that the rate of such transitions increases dramatically with decreasing levels of the key transcription factors involved (Warren and ten Wolde 2005). Indeed, *(ΔHD)p::che-1* animals showed lower CHE-1::GFP fluorescence, corresponding to 190±70 CHE-1 proteins/cell (Fig. 7E, S5B) and decreased *che-1* mRNA levels, with 1±1 mRNAs/cell in L1 larvae (Fig. 7C). In addition, CHE-1::GFP expression was lost more often and earlier in development in ASEL neurons (Fig. 7B,E), which have lower average *che-1* mRNA and protein copy numbers than ASER neurons (Fig. 2D,F). Altogether, these results point to homeodomain proteins, that bind the HD-TF binding site, as essential for long-term maintenance of *che-1* expression and thus ASE cell fate, likely by protecting the ON state against low CHE-1 copy number fluctuations.

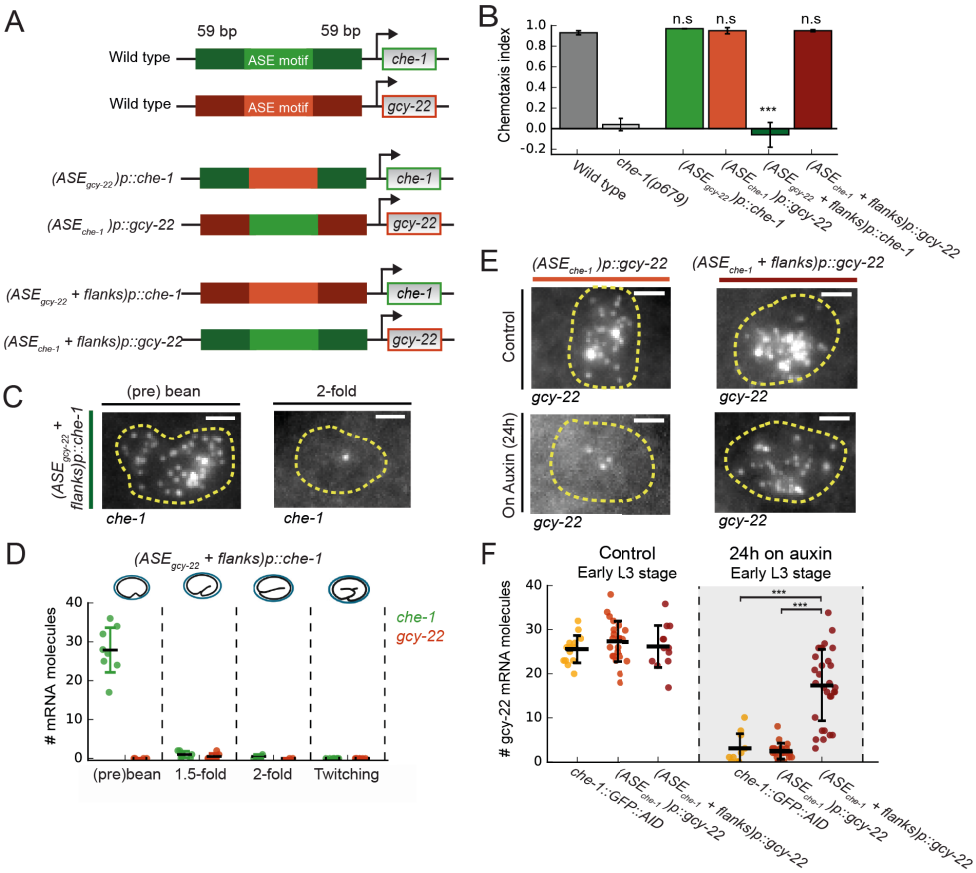

Figure 6. Region flanking CHE-1 binding site ensures resilience to CHE-1 depletion (A) Overview of *che-1* promoter mutants generated in the *che-1::GFP:AID* background. We exchanged either the *che-1* (green) or *gcy-22* (red) ASE motif, which binds CHE-1, or a larger region that includes 59 bp flanks on either side. **(B)** Average chemotaxis index for response to 10 mM NaCl, of wild-type and *che-1(p679)* animals, and *che-1* promoter mutants. Exchange of ASE motifs between *che-1* and *gcy-22* promoters did not affect chemotaxis. Replacing the *che-1* ASE motif with flanks for that of *gcy-22* abolished chemotaxis to NaCl; the reverse had no effect. **(C)** *che-1* expression visualized by smFISH in ASE neurons of *(ASE$_{gcy-22}$+flanks)p::che-1* embryos. In 2-fold embryos, *che-1* mRNA levels were low. Scale bar: 1.5 µm. **(D)** *che-1* and *gcy-22* mRNA levels quantified in the ASE neurons of *(ASE$_{gcy-22}$+flanks)p::che-1 embryos*. After initial high *che-1* expression at the time of ASE specification, *che-1* and *gcy-22* expression was almost absent, indicating a failure of ASE fate maintenance. **(E)** *gcy-22* expression under normal conditions or upon CHE-1 depletion by auxin, in L3 larvae of *che-1* promoter mutants. Scale bar: 1.5 µm. **(F)** Quantification of *gcy-22* mRNA levels upon auxin-induced CHE-1 depletion, in *gcy-22* promoter mutants. In *(ASE$_{gcy-22}$)p::che-1 animals*, *gcy-22* mRNA levels fell on auxin, as observed before. However, in *(ASE$_{che-1}$+flanks)p::gcy-22)* animals treated with auxin *gcy-22* levels remained high. Thus, the region flanking the *che-1* ASE motif drives the maintenance of *che-1* expression during CHE-1 protein depletion. Error bars in B represent mean ± S.E.M, D and F represent mean ± SD. n≥10. ***P<0.001.

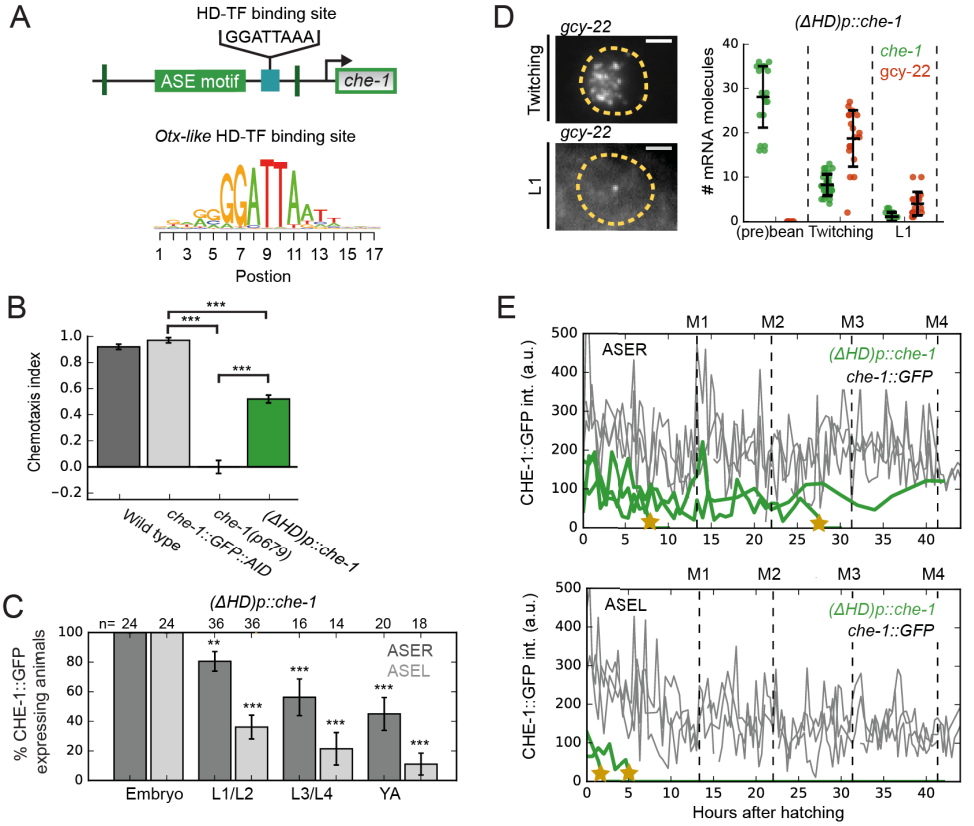

Figure 7. An Otx-like homeodomain transcription factor binding site involved in long-term maintenance of ASE cell fate. (A) Position of an *Otx*-like homeodomain transcription factor (HD-TF) binding site in the *che-1* promoter. Green lines indicate the positions of the 59 bp flanks surrounding the ASE motif. HD-TF binding site depicted as a sequence logo. The HD-TF binding site is deleted in *(ΔHD)p::che-1* animals. **(B)** Average chemotaxis index for response to 10 mM NaCl, of wild-type, *che-1::GFP::AID* and *che-1(p679)* animals, and *(ΔHD)p::che-1* mutant. Deleting the HD-TF binding site caused a decreased response to NaCl. **(C)** Fraction of *(ΔHD)p::che-1* animals expressing CHE-1::GFP in ASER (dark grey) and ASEL (light grey) at different developmental stages. CHE-1::GFP is progressively lost during development. **(D)** *che-1* and *gcy-22* mRNA levels in *(ΔHD)p::che-1* animals quantified by smFISH. Expression was similar to wild-type until late-stage, twitching embryos, but fell rapidly in newly-hatched L1 larvae. Scale bar: 2 µm. **(E)** CHE-1::GFP expression dynamics in single *che-1::GFP* (grey) and *(ΔHD)p::che-1* (green) animals during larval development. Approximate timing of molts is indicated M1-M4. CHE-1::GFP expression in *(ΔHD)p::che-1* animals was lost in a rapid and stochastic manner, at different times during development. Error bars represent S.E.M (B,D) or S.D. (C). n≥10. **P<0.01, ***P<0.001.

DISCUSSION

The terminal selector gene *che-1* controls subtype determination of the salt-sensing ASE neurons, by inducing the expression of hundreds of ASE-specific target genes while also inducing its own mRNA expression via autoregulation (Etchberger et al., 2007). It is an open question whether the positive autoregulation of CHE-1 is sufficient to maintain its own expression and, hence, ASE subtype, for the animal's entire lifetime, or whether additional mechanisms are necessary to lock in cell identity in an irreversible manner. Here, we show that transient depletion of CHE-1 is sufficient to permanently lose ASE function, indicating that *che-1* expression forms a reversible, bistable switch. This also raised the question how, in the presence of the inherent molecular fluctuations in the cell, this switch maintains its ON state (*che-1* expression) and prevents spontaneous transitions to the OFF state (no *che-1* expression).

Theoretical studies found that the stability of bistable genetic switches against fluctuations is enhanced by increasing the copy number and lifetime of the transcription factors that form the switch (Warren and ten Wolde, 2005; Walczak et al., 2005; Mehta et al., 2008). However, our simulations using *in vivo* measured *che-1* mRNA and protein copy numbers and lifetimes suggest that these values by themselves are not sufficient to generate a stable ON state. Instead, our simulations suggested a novel mechanism required to stabilize the ON state, which uses the reservoir of CHE-1 proteins bound to its many target sites to buffer *che-1* expression against fluctuations in CHE-1 level. Crucial to this target reservoir buffering mechanism is that CHE-1 exhibits strong preferential binding to its own promoter compared to its other targets. In this case, when CHE-1 protein levels drop, any CHE-1 protein that dissociates from a target gene promoter will immediately bind the *che-1* promoter, if it is found unoccupied. This ensures maintenance of *che-1* expression, at the expense of expression of its other targets, to bring CHE-1 protein levels back to the normal steady state level. Our experimental observations support this mechanism. Most importantly, upon transient CHE-1 depletion *in vivo*, expression of the CHE-1 target *gcy-22* rapidly and strongly decreased, yet *che-1* expression itself was hardly affected. We show that this resilience of *che-1* expression to CHE-1 depletion could be conferred onto other target genes by introducing a 130 bp fragment of the *che-1* promoter that surrounds the ASE motif bound by CHE-1, but not the ASE motif itself.

Target reservoir buffering relies on CHE-1 being preferentially recruited to the *che-1* promoter. We found evidence that homeodomain transcription factors are responsible for this. Deleting a HD-TF binding site close to the *che-1* ASE motif and specific to the *che-1* promoter, caused spontaneous transitions to the OFF state, and loss of cell identity, long after ASE subtype determination. This lack of stability was accompanied by lower *che-1* mRNA and protein levels, consistent with reduced recruitment of *che-1* to its own promoter. We speculate that HD-TFs act by increasing the residence time of CHE-1 at the *che-1* promoter.

Our simulations showed that highly stable ON states require a relatively small, 10-100 fold increase in CHE-1 residence time at the *che-1* promoter compared to its other targets, within the range expected if CHE-1 and a HD-TF interact cooperatively with a weak interaction of a few kBT. A similar interaction was postulated for the homeodomain protein ALR-1 in mechanosensory TRN neurons, where it restricts variability in expression of the terminal selector gene *mec-3*, by binding close to the MEC-3 binding site on its promoter (Topalidou and Chalfie, 2011). The only protein with high predicted affinity to the HD-TF binding site in the *che-1* promoter, and expressed in ASE neurons, is the OTX-like homeodomain transcription factor CEH-36 (Lanjuin et al., 2003). However, a *ceh-36* loss-of-function mutant (Chang et al., 2003) did not reproduce the loss of ASE identity seen upon deletion of the homeodomain binding site (data not shown), indicating a role for other ASE-expressed homeodomain proteins, potentially in combination with CEH-36. In general, homeodomain proteins play an important role in development of the nervous system, that is conserved from *C. elegans* to mammals (Hobert 2010; Hench et al., 2015). Our work now extends this role also to long-term maintenance of cell fate in the face of stochastic fluctuations.

The observed resilience of *che-1* expression to CHE-1 depletion is crucial for stable maintenance of ASE identity. In both our models with and without cooperativity, this is achieved by a very low threshold for inducing *che-1* expression, with a single *che-1* mRNA potentially sufficient to induce the ON state. Indeed, the recovery of CHE-1::GFP expression after 24-48 hours of CHE-1 depletion demonstrates that the ON state can be recovered from very low CHE-1 levels. However, this raises the question how stochastic, spontaneous induction of che-1 expression and ASE fate is prevented in non-ASE cells. In most cells, spontaneous induction of the ON state is likely prevented by chromatin remodelling (Tursun et al., 2011; Patel and Hobert 2017). However, transient *che-1* expression induced long-term expression of CHE-1 targets in non-ASE head sensory neurons, suggesting that these cells are capable of inducing the ON state (Tursun et al., 2011). A potential mechanism to prevent ectopic induction of the ON state is provided by our observation that preferential binding of CHE-1 to its own promoter likely depends on homeodomain proteins. Cells lacking these proteins would have difficulty inducing and maintaining *che-1* expression. Consistent with this hypothesis, a large number of HD-TFs is expressed in the *C. elegans* nervous system in a highly neuron-specific manner (Hobert, 2010). Our work suggests that cell-specific expression of co-factors of terminal selector genes might form a general mechanism to prevent spontaneous induction of these genes in the wrong cells.

While bistability in genetic networks is recognized as an important mechanism to generate cell fate switches (Ferrell, 2002), long-term cell fate maintenance is often assumed to require additional feedback mechanisms, for instance through histone and chromatin modifications, that make cell fate essentially irreversible. Here, we show that bistability through an autoregulatory feedback loop alone is sufficient for life-long maintenance of neuron identity in *C. elegans*, despite strong stochastic molecular fluctuations in the underlying

genetic network. The mechanism responsible for this depends crucially on the single-input module topology of the network, with a terminal selector gene, *che-1*, inducing both its own expression and that of many other target genes. Single-input modules are highly prevalent network motifs for neuron subtype determination, both in *C. elegans* and higher organisms (Hobert and Kratsios, 2019). In addition, cell differentiation in general is often controlled by a small number of master regulators that, directly or indirectly, induce both their own expression and that of many cell fate-specific target genes. Hence, we expect target reservoir buffering to play an important, general role in explaining stable long-term maintenance of cell fate in a broad array of systems.

Our work also underscores the link between biophysical parameters, such as molecular copy number and half-life, and stable cell fate maintenance. In mammals, stable maintenance of (neuronal) cell fate is even more challenging, given that the number of cells and their required lifetime is vastly larger compared to *C. elegans*. It will be important to determine if simply increasing copy number and half-life of a mammalian terminal selector is already sufficient, when coupled with target reservoir buffering, to explain the exceeding stability of cell fate in mammals. Our work now provides an experimental and theoretical framework to address this question.

METHODS

C. elegans strains and handling

The following alleles were used in this study: *che-1(ot856[che-1::GFP])* (kindly provided by Dylan Rahe from the Hobert lab) (Leyva-Diaz and Hobert, 2019), *gcy-5(ot835[gcy-5::SL2::mNeonGreen]*) II; o*tTi6[hsp16-41p::che-1::2xFLAG] X, che-1(p679), ieSi57[Peft-3::TIR1::mRuby::unc-54 3'UTR, Cbr-unc-119(+)]* II. A complete list of strains used in this study, including transgenic strains generated by CRISPR/Cas9, is available upon request.

The wild-type strain used was the *C. elegans* variety Bristol, strain N2. All *C. elegans* strains were maintained on Nematode Growth Medium (NGM) plates, containing *E. coli* strain OP50 as a food source, at 20°C (Brenner, 1974), unless indicated otherwise. Worms were maintained according to standard protocol.

CRISPR/Cas9-mediated genome editing

Genome editing was performed according to protocol (Dokshin et al., 2018) and using ssODN repair templates with 35 bp homology arms (Paix et al., 2017). An AID tag was endogenously inserted at the C-terminus of GFP in a *che-1(ot856[che-1::GFP])* background using guide g2 and a repair template containing the degron sequence (Zhang et al., 2015), generating *che-1(gj2089[che-1::GFP::AID])*. Subsequently, the *ieSi57* allele (Zhang et al., 2015) was introduced. All *che-1* or *gcy-22* promoter mutations were made in this *che-1(gj2089[che-1::GFP::AID];ieSi57* background. *(ASE_{gcy-22}+flanks)p::che-1* was generated using a template containing the ASE motif of the *gcy-22* promoter and its 59 bp flanking regions, and guides g51 and g52. *(ASE_{che-1}+flanks)p::gcy-22* was generated using a template containing the ASE motif of *che-1* and its 59 bp flanks and guides g55 and g56. *(ASE_{gcy-22})p::che-1* was generated using a template containing the ASE motif of *gcy-22* and guide g53. *(ASE_{che-1})p::gcy-22* was generated using a template containing the ASE motif of *che-1* and guide g57. *(ΔHD)p::che-1* was generated using a template containing the 5 bp flanks of the HD motif from the promoter of *che-1* and guide g54. Guides and ssODNs used in this research are listed in Table S4, available upon request.

Single Molecule Fluorescence In Situ Hybridization (smFISH)

The oligonucleotides for the smFISH probe sets were designed with optimal GC content and specificity for the gene of interest using the Stellaris RNA FISH probe designer. The oligonucleotides were synthesized with a 3' amino C7 modification and purified by LGC Biosearch Technologies. Conjugation of the oligonucleotides with either Cy5 (GE Amersham) or Alexa594 (Invitrogen) was done as previously described (Lyubimova, 2013). Sequences of each probe set are listed in Table S3 (with exception of *gcy-14*) and are available upon request. The smFISH protocol was performed as previously described (Raj et al., 2008; Ji and van Oudenaarden 2012). Briefly, staged animals were washed from plates with M9 buffer and fixed in 4%

formaldehyde in 1x PBS, gently rocking at room temperature (RT) for 40 minutes (young adults for 35 minutes). Fixation of embryos required a snap-freeze step to crack the eggshells by submerging embryos, after 15 minutes in fixation buffer, in liquid nitrogen, and thawing on ice for 20 minutes. After fixation, the animals were 2x washed with 1xPBS and resuspended in 70% ethanol overnight at 4°C. Ethanol was removed and animals were washed with 10% formamide and 2X SSC, as preparation for the hybridization. Animals were incubated with the smFISH probes overnight in the dark at 37°C in a hybridization solution (Stellaris) with added 10% formamide. The next day, animals were washed 2x with 10% formamide and 2X SSC each with an incubation step of 30 minutes at 37°C. The last wash step contains DAPI 5 µg/mL for nuclear staining. The wash buffer was removed, and animals were resuspended in 2X SSC and stored at 4°C until imaging. The 2X SSC was aspirated and animals were immersed in 100 µl GLOX buffer (0.4% glucose, 10 mM Tris-HCl, pH 8.0, 2X SSC) together with 1 µl Catalase (Sigma-Aldrich) and 1 µl glucose oxidase (Sigma-Aldrich) (3.7 mg/mL) to prevent bleaching during imaging.

Microscopy images of smFISH samples were acquired with a Nikon Ti-E inverted fluorescence microscope, equipped with a 100X plan-apochromat oil-immersion objective and an Andor Ikon-M CCD camera controlled by µManager software (Edelstein et al., 2014). smFISH analysis was performed with custom Python software, based on a previously described method (Raj et al., 2008). Briefly, we first convolved the smFISH images with a Gaussian filter. Next, candidate spots were selected via manual thresholding, and partially overlapping spots were separated via finding 3D regional intensity maxima. We used the spatial localization of *gcy-22* or *gcy-14* mRNA molecules which are highly expressed ASE-specific genes, to estimate the cell boundaries of the ASE neurons. The coverage of the ASE cell bodies with *gcy-22* or *gcy-14* mRNA molecules agreed with GFP markers (*gcy-5p::GFP* or *gcy-7p::GFP*) that marked the cell body.

CHE-1 protein quantification

Staged *che-1::GFP* knock-in animals were bathed in 72 nM and 48 nM eGFP recombinant protein (Bio-connect) with 0.25 mM Levamisole (Sigma-Aldrich) in M9 buffer in a glass chambered cover glass systems (IBL baustoff), which were coated with 0.5 mg/ml kappa-capsein in the buffer MRB80 (80 mM Pipes, 4 mM $MgCl_2$, 1 mM EGTA, pH 6.8 with KOH) to prevent binding of eGFP to the cover glass and chamber walls. Images of bathed *che-1::GFP* animals in eGFP solution were acquired with a Nikon Eclipse Ti inverted microscope, equipped with a Nikon C1 confocal scan head, a 100 mW Argon ion laser (488nm, Coherent), and a S Fluor 40×1.3 NA and an Apo TIRF 100×1.49 NA objective. Calibration of eGFP with *che-1::GFP* animals was repeated 2 times at different days with 72 nM and 48 nM eGFP concentrations, of which we took the average calibration measurements. For ease of measuring, the CHE-1::GFP signal of animals was measured with the exact same microscope and software settings, except placing the animals submersed in 0.25 mM Levamisole (Sigma-Aldrich) in M9 buffer on agar

pads with the same cover glass thickness on top. The ASE neuron closest to the cover glass was imaged in larvae to circumvent tissue scattering. Embryos were followed in time (at 22°C) and imaged every 20 minutes with the exact same microscope and software settings, from bean stage until twitching started. For both larvae and embryos, the slices focused at the approximate middle of the ASE neuron nuclei were used for quantifying the CHE-1::GFP signal. The volumes of the nuclei were calculated by measuring the radii of the nuclei in x, y and z direction from the CHE-1::GFP signal with the assumption that the nucleus shape resembles a ellipsoid, using the following equation: $V = {}^{4}/_{3}\pi xyz$.

FRAP

To estimate the protein degradation rate of CHE-1::GFP, we used Fluorescence Recovery After Photobleaching (FRAP). Animals were immobilized using Polybead microspheres (Polyscience) in M9 buffer on agarose pads covered with a cover glass. To prevent dehydration of animals, the coverslip was sealed with VALAP (vaseline, lanolin and paraffin, ratio 1:1:1). Animals were monitored at several time points during the experiment if they were still alive by checking very subtle movement and/or pumping behaviour. The GFP signal in the ASE neurons of the animals was bleached until approximately 20% of the initial signal was left. After bleaching, the GFP signal was measured every 20 or 30 minutes until the signal had recovered. Images were taken with the same microscope as in the CHE-1 protein quantification section. We measured for each time point the average GFP intensity in the ASE neurons and subtracted the background intensity measured nearby the ASE neurons. The degradation rate was calculated from the initial slope of the growth curve using the following exponential model: $R(t) = \left(\frac{f}{b}\right) + \left(x_0 - \left(\frac{f}{b}\right)\right)e^{-bt}$, where x_0 is the initial fluorescent intensity at the start of the recovery curve right after bleaching. *b* and *f* represent the CHE-1 protein degradation and production rate, which are fitted on the individual measured recovery curves, to obtain the average CHE-1 protein degradation rate.

che-1 mRNA stability

We induced *che-1* mRNA overexpression with the *otTi6* [*hsp16-41p::che-1::2xFLAG*] X inducible heat shock strain, and we quantified with smFISH *che-1* mRNA in the ASER neurons in L2 larvae over time (t_i=0, … ,4) ~17 min apart until recovery. We determined the relative amount of che-1 mRNAs from the start of the measurement, $n(t_i) = \frac{N(ti) - N_{control}}{N_{HS} - N_{control}}$, where $N_{control}$ is the calculated average amount of *che-1* mRNAs when there is no *che-1* mRNA overexpression, N_{HS} the calculated average amount of *che-1* mRNAs at the first measured time point right after heat shock induction, and *n(t)* is the amount of *che-1* mRNAs at the three remaining time points. An exponential degradation curve e^{-at} was fitted to the experimentally determined values $n(t_i)$, to obtain the approximate *che-1* mRNA degradation rate.

Mathematical Model of the CHE-1 switch

The cooperative mathematical model assumes that CHE-1 protein (*C*) has to bind as a dimer on the *che-1* promoter to induce *che-1* mRNA expression. The binding and unbinding of the two CHE-1 proteins at the *che-1* promoter (*O*) is separated into two events, first one CHE-1 binds with binding rate f_O and unbinds with unbinding rate b_1 from the *che-1* promoter (*OC*). When the first CHE-1 protein is bound to the *che-1* promoter, the second CHE-1 protein binds with the same binding rate f_O next to the first CHE-1, forming a dimer on the *che-1* promoter (*OC2*), and unbinds with the unbinding rate b_2. CHE-1 proteins bind as a monomer on the target gene promoters (O_TC), with the unbinding rate b_T, and with same the binding rate f_O as on the *che-1* promoter. *che-1* mRNA (*M*) is transcribed with the production rate f_M only when two CHE-1 proteins are bound to the *che-1* promoter, and *che-1* mRNA is translated into CHE-1 protein with the protein production rate f_c. Both *che-1* mRNA and CHE-1 protein are degraded with the degradation rates, b_M and b_C respectivily. This leads to the following differential equations:

$$\frac{dOC}{dt} = f_O\big(O^* - (OC + OC2)\big)C - b_1 OC$$

$$\frac{dOC2}{dt} = f_O OC \cdot C - b_2 OC2$$

$$\frac{dO_TC}{dt} = f_O(O_T^* - O_TC)C - b_T O_T \cdot C$$

$$\frac{dM}{dt} = f_M OC2 - b_M M$$

$$\frac{dC}{dt} = -f_O\big(O^* - (OC + OC2)\big)C - f_O OC \cdot C - f_O(O_T^* - O_TC)C + b_1 OC + b_2 OC2 + b_T O_T \cdot C + f_c M - b_C C$$

Where O^* is the total number of *che-1* promoters and where O^*_T is the total number of target genes.

In the non-cooperative model, CHE-1 binds (f_O) and unbinds (b_O) as a monomer on the *che-1* promoter (*OC*) and induces *che-1* expression as a monomer. The other reactions in the model are the same as in the cooperative model. This leads to the following differential equations:

$$\frac{dOC}{dt} = f_O(O^* - OC)C - b_O OC$$

$$\frac{dO_TC}{dt} = f_O(O_T^* - O_TC)C - b_TO_T \cdot C$$

$$\frac{dM}{dt} = f_MOC - b_MM$$

$$\frac{dC}{dt} = -f_O(O^* - OC)C - f_O(O_T^* - O_TC)C + b_OOC + b_TO_T.C + f_cM - b_CC$$

Bistability

In the cooperative model CHE-1 proteins bind as a dimer at the *che-1* promoter to induce *che-1* expression. The binding of two CHE-1 proteins in the system, implies non-linear behaviour, giving rise to bistability. We have in the cooperative model three fixed points, 2 stable and 1 unstable fixed point. The 2 stable fixed points represent the so-called "ON state" (high CHE-1) and the "OFF state" (low CHE-1) of the CHE-1 switch. When the switch is in the OFF state, it has to cross the unstable point to reach the ON state. In contrast, the non-cooperative model, in which CHE-1 proteins bind as a monomer at the *che-1* promoter to induce *che-1* expression, has only two fixed points. The first fixed point represents the ON state, in which CHE-1 protein levels are high. The second fixed point is a half-stable point, when there is no CHE-1 protein, the switch is OFF. However, the introduction of, for example, only 1 *che-1* mRNA in the system would be sufficient to turn the switch from the OFF state to the ON state.

Simulations

To study the short-term lifetime (<1 weeks) of the cooperative and non-cooperative CHE-1 switch, we performed stochastic Gillespie simulations on both models (Gillespie 1977). We used a custom written python script to simulate the reactions involved in both CHE-1 switch models. All reactions describing the differential equations from the cooperative and non-cooperative model, are summarized in Fig. 3A. Parameters remain unchanged during simulations (with exception for transient depletion simulations) and species are initiated in the ON state.

To study ON state lifetimes of the CHE-1 switch exceeding 1 weeks, in the cooperative and non-cooperative CHE-1 switch model, we used Forward Flux Sampling (Allen et al., 2006; Allen et al., 2009), a computational method which allowed us to estimate lifetimes of CHE-1 switches. It was not necessary to integrate pruning into the algorithm since this would not result in improvement in computational efficiency. The FFS algorithm was initiated with the same initial conditions as the Gillespie simulations. Interfaces of the FFS algorithm were chosen according to the variance of CHE-1 protein in the ON state, to generate a 5-10%

chance of CHE-1 protein trajectories crossing the first interface (with an exception for very unstable switch, where CHE-1 protein simulations immediately run to the OFF state). The typical step size of the interfaces was 20 and the number of interfaces was between 20 and 35.

Parameters

We can divide the parameters in the following groups: 1.) experimentally determined parameters, 2.) parameters that we could approximate, 3.) unconstrained parameters and 4.) parameters that we could calculate with help of the other parameters. First, the parameters which were experimentally determined. We based the *che-1* mRNA degradation rate (b_M) on direct measurement of *che-1* mRNA degradation that we quantified in the ASER neuron (Fig 2A-B). We used an approximation of *che-1* mRNA lifetime of 20 minutes. The amount of CHE-1 protein *C* was set to 900 molecules (average of ASER and ASEL at L4/YA stage) based on the CHE-1 protein quantification experiments, and the amount of *che-1* mRNAs (*M*) was set to 7 molecules (average of ASER and ASEL at L4 stage) based on the smFISH experiments in wild-type animals.

The binding rate of CHE-1 at its own promoter f_O and the target gene promoters f_O is approximated by the diffusion limited binding rate. The diffusion limited binding rate of CHE-1 on promoter sites was calculated using the following diffusion equation: $f_D = 4\pi\sigma D$, where reaction cross section $\sigma = 1 \cdot 10^{-2}\ \mu m$, i.e. the size of the promoter binding site, and the diffusion coefficient constant is $D = 1\ \mu m^2\ s^{-1}$. To obtain the diffusion coefficient that we can apply in our simulations, which includes information about the volume of the nucleus, the diffusion coefficient f_D was divided with the average nucleus volume (V_C) of 4 µm^3 in ASER and ASEL, resulting in a diffusion limited binding rate of $f_O = \frac{f_D}{V_C} = 0.03\ s^{-1}$.

To approximate the number of target sites where the CHE-1 protein can bind, we used the crude approximation depicted from the study of Etchberger et al. (2007), in which they found 596 genes represented with at least three times as many tags in the ASE versus AFD SAGE library, which is expected to contain almost no "false positives". We acquired the total amount of ASE motifs (minimum score of 98%) in each of the promoter regions (<1000 bp upstream of the start site) with a custom written R script, using the TFBSTools/JASPAR2018 packages, resulting in a total of 425 ASE motifs. However, the data set lacked, for example, housekeeping genes expressed in the ASE neurons that could be under control of *che-1*. The sci-RNA-seq dataset from the study of Cao et al. (2017), provides information on genes expected to be expressed in the ASE neurons, including ASE non-specific genes (Cao et al., 2017). A total of 1400-1500 genes are expected to be expressed in the ASEL and ASER (score >100, removal of "false-positives"), resulting in ~1000 ASE motifs on which CHE-1 could potentially bind. In the simulations we used either 500 or 1000 target sites.

The unbinding rates of CHE-1 from its own promoter and the target gene promoters, b_1, b_2, b_T are the only unconstrained parameters, and are ranged between 0.1 and 100 sec^{-1} in the FFS simulations. The CHE-1 protein degradation rate b_C, the CHE-1 production rate f_C and the *che-1* mRNA production rate f_M are dependent on the unbound fraction of CHE-1 protein. To calculate the three unknown rates b_C, f_C, f_M first the CHE-1 protein degradation rate b_C was set at the experimentally measured parameter, and used to calculate the *che-1* mRNA production rate f_M and CHE-1 protein production rate f_C. The CHE-1 production rate is influenced by the amount of CHE-1 bound at the target gene promoters, hence why the CHE-1 protein production and degradation had to be fitted to the experimentally measured CHE-1 protein FRAP curve. The fitting was done by introducing CHE-1::GFP species, bleached or unbleached, in the existing model in order to reproduce in simulation the FRAP experiments. The bleached CHE-1::GFP proteins could also bind and unbind the promoters and induce *che-1* expression, but the bleached CHE-1::GFP proteins could not be produced, only degraded.

In the table below, we summarize all parameter values. In this table, all parameter values are defined for the *Unstable CHE-1 switch* (4B), and the other model parameter values are only given when they deviate from those used in the *Unstable CHE-1 switch* (4B).

The parameters for the depletion simulations panel (Fig 4E) include an extra promoter (*PO*) with production and degradation rates of (*PM*) mRNA, b_p, f_p to simulate the production of target mRNA induced by CHE-1. The binding and unbinding rates of the extra promoter are the same as for the target genes, f_O, b_T.

Estimation of required ON state lifetime.
If spontaneous switches from the ON to the OFF state occur as a Poisson process with rate r, then the probability of a switching event occurring at time t is given by the exponential distribution $p(t) = r\exp(-rt)$. The fraction of animals in which a switching event occurs before time $t=T$ is given by the cumulative distribution $P(t) = 1 - \exp(-rt)$. This fraction is smaller than a value ϕ if $r < -\ln(1-\phi)/T$. For small fractions $\phi \approx 0$, this can be approximated as $r < \phi/T$. If a switching event can occur only in 1 out of 10^6 animals, $\phi = 1 \cdot 10^{-6}$, within the average animal lifetime of $T=2$ weeks, then the required life time of the ON state is given by $1/r > 2.3 \cdot 10^5$ years.

Parameter	Description	Value
Unstable swith (4b)	Unstable CHE-1 switch, average lifetime ~10 days	
C	Number of CHE-1 protein molecules	900
M	Number of *che-1* mRNA molecules	7
O_S	Number of *che-1* promoters	1
O_{T_S}	Number of target genes	500
f_O	Binding rate of CHE-1 on *che-1* or target gene promoters	0.03 sec^{-1}
b_O	Unbinding rate of CHE-1 from *che-1* promoter	100 sec^{-1}
b_T	Unbinding rate of CHE-1 from target gene promoters	100 sec^{-1}
f_M	*che-1* mRNA production rate	0.0302 sec^{-1}
b_M	*che-1* mRNA degradation rate	0.00083 sec^{-1}
f_C	CHE-1 protein production rate	0.0274 sec^{-1}
b_c	CHE-1 protein degradation rate	0.00024 sec^{-1}
Stable swith (4b)	Highly stable switch, slower unbinding rate of CHE-1 from its own promoter	
b_O	Unbinding rate of CHE-1 from *che-1* promoter	0.1 sec^{-1}
f_M	*che-1* mRNA production rate	0.0059 sec^{-1}
f_c	CHE-1 protein production rate	0.0261 sec^{-1}
b_c	CHE-1 protein degradation rate	0.00023 sec^{-1}
Stable switch (4E)	Highly stable switch, depleted to 100 CHE-1	
b_O	Unbinding rate of CHE-1 from *che-1* promoter	0.1 sec^{-1}
f_M	*che-1* mRNA production rate	0.0059 sec^{-1}
b_C	CHE-1 protein degradation rate	0.0019 sec^{-1}
f_C	CHE-1 protein production rate	0.024 sec^{-1}
b_P	Target mRNA degradation rate	0.0008 sec^{-1}
f_P	Target mRNA production rate	0.09 sec^{-1}
Unstable switch (4E)	Unstable switch, depleted to 100 CHE-1	
b_O	Unbinding rate of CHE-1 from *che-1* promoter	10 sec^{-1}
b_T	Unbinding rate of CHE-1 from target gene promoters	10 sec^{-1}
b_C	CHE-1 protein degradation rate	0.00076 sec^{-1}
f_C	CHE-1 protein production rate	0.026 sec^{-1}
b_P	Target mRNA degradation rate	0.0004 sec^{-1}
f_P	Target mRNA production rate	0.016 sec^{-1}

Auxin induced protein degradation

The Auxin Inducible Degron (AID) System was employed as previously described (Zhang et al., 2015). Animals were initially grown on NGM plates with OP50 without IAA (Sigma-Aldrich). To induce degradation of CHE-1, L1 staged animals were transferred to NGM plates with OP50 and 1 mM IAA in EtOH at 20 °C.

For the CHE-1::GFP::AID measurements, the duration of auxin exposure and recovery were varied in each treatment. The animals were transferred every other day to new NGM plates with 1 mM IAA or recovery NGM plates without IAA to prevent mixing of generations. Each treatment contained a control group of *che-1::GFP::AID* animals never exposed to auxin. For imaging, the animals were placed on an 5% agarose pad submerged in 0.25 mM Levamisole (Sigma-Aldrich) in M9 with a cover glass on top. We checked for CHE-1::GFP::AID in the ASE neurons with a wide field microscope. Older animals showed stronger autofluorescence in the head, giving rise to nuclei-like structures which could be confused with ASE neurons. The GFP (FITC) channel was combined with the TRITC channel to correct for the autofluorescence (Teuscher and Ewald, 2018). Due to tissue scattering and decrease in CHE-1::GFP signal in old animals, we found the ASE neuron closest to the cover glass was most reliable. The control group always showed CHE-1::GFP::AID in the ASE neurons: even though CHE-1::GFP::AID levels decreased with age, even 10 days old animals had well identifiable ASE neurons.

NaCl chemotaxis assay

The quadrant assay used to asses chemotaxis to NaCl was adapted from Wicks et al. (2000) and Jansen et al. (2002). Briefly, two diagonally opposite quadrants of a sectional petri dish (Star Dish, Phoenix Biomedical) were filled with 13.5 ml buffered agar (1.7% Agar, 5 mM K_2HPO_4/KH_2PO_4 pH 6, 1 mM $CaCl_2$ and 1 mM $MgSO_4$) containing NaCl and two diagonally opposite quadrants with 13.5 ml buffered agar without NaCl. Immediately before the assay, the plastic dividers between the quadrants were covered with a thin layer of agar. Age synchronized *C. elegans* populations, cultured at 25°C for ~66 hours, were washed 3 times for 5 min. with CTX buffer (5 mM K_2HPO_4/KH_2PO_4 pH 6, 1 mM $CaCl_2$ and 1 mM $MgSO_4$). Approximately 100 animals were placed in the middle of a sectional dish. After 10 min., animals on each quadrant were counted and a chemotaxis index (CI) was calculated for each plate (CI = (# animals on NaCl – # animals not on NaCl)/ total # animals). To determine the CI of a strain, 2 assays per day were performed on at least 2 different days.

To assess the effect of CHE-1 depletion on chemotaxis, animals were bleached and cultured for 24 hours on NGM plates without IAA at 20°C. After 24 hours animals were transferred to NGM plates containing 1 mM IAA. To remove eggs and larvae, animals were thoroughly rinsed using CTX buffer and a 30 µm pluriStrainer (pluriSelect) and transferred to a fresh NGM plate, with or without 1 mM IAA, starting at 96 hours into the experiment and repeated every 24 hours until the end of the experiment. After the experimental treatment duration, the chemotaxis index (CI) was determined. Subsequently, recovery was started by transferring animals to NGM plates without IAA and the CI was determined 24 hours and 48 hours thereafter. At each timepoint, the CI was determined in similarly aged *che-1(p679)* and untreated c*he-1::GFP::AID* animals.

Time lapse

Time-lapse imaging was performed as previously described (Gritti et al., 2016). Briefly, micro-chambers are made out of polyacrylamide hydrogel, made from a 10% dilution of 29:1 acrylamide/bis-acrylamide (Sigma-Aldrich) was mixed with 0.1% ammonium persulfate (Sigma-Aldrich) and 0.01% TEMED (Sigma-Aldrich) as polymerization initiators. For the time-lapse experiments the chambers were 240x240x20 µm, these dimensions were sufficient to contain enough OP50 bacteria to sustain development until animals started laying eggs.

We used a Nikon Ti-E inverted microscope with a 40x objective in all experiments. The microscope has a Hamamatsu Orca Flash 4.0 v2 camera set at full frame and full speed. The camera chip is 13x13 mm and contains 4Mp. We used 488 nm lasers (Coherent OBIS-LS 488-100) for fluorescence excitation. We used a high fluorescent signal of 100 mW with an exposure time of 10 ms, since the fluorescent signal of CHE-1::GFP is relatively low. To keep track of the molting cycle as indication of the age of the animals, we used bright field imaging, which contained a red LED (CoolLED, 630nm). Time-lapse images were acquired every 20 minutes without detectable phototoxicity effects.

Images were analyzed with custom written time-lapse software, and with ImageJ. Briefly, first we corrected the raw images for experimental aberrations with flat and dark field images acquired at the end of the experiment. For quantification purposes, we computed the average fluorescence of each ASE neuron via drawing a region of interest around each nucleus and we corrected the average intensity by subtracting the background level close to the ASE neuron.

Quantification and statistical analysis

Image analysis of CHE-1::GFP quantification and intensity measurements was performed with the ImageJ distribution Fiji (Schindelin et al., 2012). For the quantification data shown in graphs of all figures, the dots represent individual values, the boxplots without box represent the mean and the standard deviation.

Statistical analyses were performed either using R software, version 3.6.0, or with Python 3.5 Package SciPy. Comparisons of the chemotaxis indexes were performed using a one-way ANOVA, followed by a pairwise t-test with Holm correction. Significance between control versus conditions in smFISH data were preformed using one-way ANOVA, followed by a Tukey multiple comparison test. Significance of the percentage of ASE neurons expressing CHE-1::GFP between treatment groups (on auxin) and control group (no auxin) was determined using Fisher exact test.

ACKNOWLEDGEMENTS

Some strains were provided by the CGC, which is funded by NIH Office of Research Infrastructure Programs (P40 OD010440), and the Mitani laboratory through the National Bio-Resource Project of the MEXT, Japan. We thank Dylan Rahe (Hobert lab) for providing the GFP-tagged che-1(ot856) allele. This work is part of the research program of the Foundation for Fundamental Research on Matter (FOM), which is financially supported by the Netherlands Organization for Scientific Research (NWO).

AUTHOR CONTRIBUTIONS

J.J.H.T, S.N.B., G.J. and J.S.Z conceived the study. J.J.H.T performed smFISH, time-lapse and (confocal) microscopy expression experiments and data analysis. S.N.B. generated strains, performed behavioural assays and data analysis. J.J.H.T and J.S.Z. performed mathematical modelling. J.J.H.T, S.N.B., G.J. and J.S.Z. wrote the manuscript.

REFERENCES

Acar, M., A. Becskei, and A. van Oudenaarden. 2005. Enhancement of cellular memory by reducing stochastic transitions, Nature, 435: 228-32.

Allen, R. J., D. Frenkel, and P. R. ten Wolde. 2006. Forward flux sampling-type schemes for simulating rare events: efficiency analysis, J Chem Phys, 124: 194111.

Allen, R. J., C. Valeriani, and P. Rein Ten Wolde. 2009. Forward flux sampling for rare event simulations, J Phys Condens Matter, 21: 463102.

Alon, U. 2007. Network motifs: theory and experimental approaches, Nat Rev Genet, 8: 450-61.

Anderson, P. 1995. Mutagenesis, Methods Cell Biol, 48: 31-58.

Brenner, S. 1974. The genetics of *Caenorhabditis elegans*, Genetics, 77: 71-94.

Cao, J., J. S. Packer, V. Ramani, D. A. Cusanovich, C. Huynh, R. Daza, X. Qiu, C. Lee, S. N. Furlan, F. J. Steemers, A. Adey, R. H. Waterston, C. Trapnell, and J. Shendure. 2017. Comprehensive single-cell transcriptional profiling of a multicellular organism, Science, 357: 661-67.

Chang, S., R. J. Johnston, Jr., and O. Hobert. 2003. A transcriptional regulatory cascade that controls left/right asymmetry in chemosensory neurons of *C. elegans*, Genes Dev, 17: 2123-37.

Coburn, C. M., and C. I. Bargmann. 1996. A putative cyclic nucleotide-gated channel is required for sensory development and function in *C. elegans*, Neuron, 17: 695-706.

Deneris, E. S., and O. Hobert. 2014. Maintenance of postmitotic neuronal cell identity, Nat Neurosci, 17: 899-907.

Dhondt, I., V. A. Petyuk, S. Bauer, H. M. Brewer, R. D. Smith, G. Depuydt, and B. P. Braeckman. 2017. Changes of Protein Turnover in Aging *Caenorhabditis elegans*, Mol Cell Proteomics, 16: 1621-33.

Dokshin, G. A., K. S. Ghanta, K. M. Piscopo, and C. C. Mello. 2018. Robust Genome Editing with Short Single-Stranded and Long, Partially Single-Stranded DNA Donors in *Caenorhabditis elegans*, Genetics, 210: 781-87.

Edelstein, A. D., M. A. Tsuchida, N. Amodaj, H. Pinkard, R. D. Vale, and N. Stuurman. 2014. Advanced methods of microscope control using muManager software, J Biol Methods, 1.

Etchberger, J. F., E. B. Flowers, R. J. Poole, E. Bashllari, and O. Hobert. 2009. *Cis*-regulatory mechanisms of left/right asymmetric neuron-subtype specification in *C. elegans*, Development, 136: 147-60.

Etchberger, J. F., A. Lorch, M. C. Sleumer, R. Zapf, S. J. Jones, M. A. Marra, R. A. Holt, D. G. Moerman, and O. Hobert. 2007. The molecular signature and *cis*-regulatory architecture of a *C. elegans* gustatory neuron, Genes Dev, 21: 1653-74.

Ferrell, J. E., Jr. 2002. Self-perpetuating states in signal transduction: positive feedback, double-negative feedback and bistability, Curr Opin Cell Biol, 14: 140-8.

Fornasiero, E. F., S. Mandad, H. Wildhagen, M. Alevra, B. Rammner, S. Keihani, F. Opazo, I. Urban, T. Ischebeck, M. S. Sakib, M. K. Fard, K. Kirli, T. P. Centeno, R. O. Vidal, R. U. Rahman, E. Benito, A. Fischer, S. Dennerlein, P. Rehling, I. Feussner, S. Bonn, M. Simons, H. Urlaub, and S. O. Rizzoli. 2018. Precisely measured protein lifetimes in the mouse brain reveal differences across tissues and subcellular fractions, Nat Commun, 9: 4230.

Gebhardt, J. C., D. M. Suter, R. Roy, Z. W. Zhao, A. R. Chapman, S. Basu, T. Maniatis, and X. S. Xie. 2013. Single-molecule imaging of transcription factor binding to DNA in live mammalian cells, Nat Methods, 10: 421-6.

Gillespie, Daniel, 1977. Exact stochastic simulation of coupled chemical reactions The journal of physical, 81: 2340-61.

Gregor, T., D. W. Tank, E. F. Wieschaus, and W. Bialek. 2007. Probing the limits to positional information, Cell, 130: 153-64.

Gritti, N., S. Kienle, O. Filina, and J. S. van Zon. 2016. Long-term time-lapse microscopy of *C. elegans* post-embryonic development, Nat Commun, 7: 12500.

Hench, J., J. Henriksson, A. M. Abou-Zied, M. Luppert, J. Dethlefsen, K. Mukherjee, Y. G. Tong, L. Tang, U. Gangishetti, D. L. Baillie, and T. R. Burglin. 2015. The Homeobox Genes of *Caenorhabditis elegans* and Insights into Their Spatio-Temporal Expression Dynamics during Embryogenesis, PLoS One, 10: e0126947.

Hobert, O. 2008. Regulatory logic of neuronal diversity: terminal selector genes and selector motifs, Proc Natl Acad Sci U S A, 105: 20067-71.

Hobert, O. 2010. Neurogenesis in the nematode *Caenorhabditis elegans*, WormBook: 1-24.

Hobert, O. 2016. Terminal Selectors of Neuronal Identity, Curr Top Dev Biol, 116: 455-75.

Hobert, O., and P. Kratsios. 2019. Neuronal identity

control by terminal selectors in worms, flies, and chordates, Curr Opin Neurobiol, 56: 97-105.

Hsiao, H. Y., D. Jukam, R. Johnston, and C. Desplan. 2013. The neuronal transcription factor erect wing regulates specification and maintenance of *Drosophila* R8 photoreceptor subtypes, Dev Biol, 381: 482-90.

Jansen, G., D. Weinkove, and R. H. Plasterk. 2002. 'The G-protein gamma subunit *gpc-1* of the nematode *C. elegans* is involved in taste adaptation', EMBO J, 21: 986-94.

Ji, N., and A. van Oudenaarden. 2012. Single molecule fluorescent in situ hybridization (smFISH) of *C. elegans* worms and embryos, WormBook: 1-16.

Jung, C., P. Bandilla, M. von Reutern, M. Schnepf, S. Rieder, U. Unnerstall, and U. Gaul. 2018. True equilibrium measurement of transcription factor-DNA binding affinities using automated polarization microscopy, Nat Commun, 9: 1605.

Lanjuin, A., M. K. VanHoven, C. I. Bargmann, J. K. Thompson, and P. Sengupta. 2003. *Otx/otd* homeobox genes specify distinct sensory neuron identities in *C. elegans*, Dev Cell, 5: 621-33.

Leblond, C. P., and B. E. Walker. 1956. Renewal of cell populations, Physiol Rev, 36: 255-76.

Leyva-Diaz, E., and O. Hobert. 2019. Transcription factor autoregulation is required for acquisition and maintenance of neuronal identity, Development, 146.

Mehta, P., R. Mukhopadhyay, and N. S. Wingreen. 2008. Exponential sensitivity of noise-driven switching in genetic networks, Phys Biol, 5: 026005.

Ming, G. L., and H. Song. 2005. Adult neurogenesis in the mammalian central nervous system, Annu Rev Neurosci, 28: 223-50.

Ninkovic, J., L. Pinto, S. Petricca, A. Lepier, J. Sun, M. A. Rieger, T. Schroeder, A. Cvekl, J. Favor, and M. Gotz. 2010. The transcription factor Pax6 regulates survival of dopaminergic olfactory bulb neurons via crystallin alphaA, Neuron, 68: 682-94.

Orlando, V. 2003. Polycomb, epigenomes, and control of cell identity, Cell, 112: 599-606.

Ortiz, C. O., S. Faumont, J. Takayama, H. K. Ahmed, A. D. Goldsmith, R. Pocock, K. E. McCormick, H. Kunimoto, Y. Iino, S. Lockery, and O. Hobert. 2009. Lateralized gustatory behavior of *C. elegans* is controlled by specific receptor-type guanylyl cyclases, Curr Biol, 19: 996-1004.

Ozbudak, E. M., M. Thattai, H. N. Lim, B. I. Shraiman, and A. Van Oudenaarden. 2004. Multistability in the lactose utilization network of *Escherichia coli,* Nature, 427: 737-40.

Paix, A., A. Folkmann, and G. Seydoux. 2017. Precision genome editing using CRISPR-Cas9 and linear repair templates in *C. elegans*, Methods, 121-122: 86-93.

Patel, T., and O. Hobert. 2017. Coordinated control of terminal differentiation and restriction of cellular plasticity, Elife, 6.

Raj, A., P. van den Bogaard, S. A. Rifkin, A. van Oudenaarden, and S. Tyagi. 2008. Imaging individual mRNA molecules using multiple singly labeled probes, Nat Methods, 5: 877-9.

Ringrose, L., and R. Paro. 2007. Polycomb/Trithorax response elements and epigenetic memory of cell identity, Development, 134: 223-32.

Sarin, S., C. Antonio, B. Tursun, and O. Hobert. 2009. The *C. elegans* Tailless/TLX transcription factor *nhr-67* controls neuronal identity and left/right asymmetric fate diversification, Development, 136: 2933-44.

Schindelin, J., I. Arganda-Carreras, E. Frise, V. Kaynig, M. Longair, T. Pietzsch, S. Preibisch, C. Rueden, S. Saalfeld, B. Schmid, J. Y. Tinevez, D. J. White, V. Hartenstein, K. Eliceiri, P. Tomancak, and A. Cardona. 2012. Fiji: an open-source platform for biological-image analysis, Nat Methods, 9: 676-82.

Schwanhausser, B., D. Busse, N. Li, G. Dittmar, J. Schuchhardt, J. Wolf, W. Chen, and M. Selbach. 2011. Global quantification of mammalian gene expression control, Nature, 473: 337-42.

Sharova, L. V., A. A. Sharov, T. Nedorezov, Y. Piao, N. Shaik, and M. S. Ko. 2009. Database for mRNA half-life of 19 977 genes obtained by DNA microarray analysis of pluripotent and differentiating mouse embryonic stem cells, DNA Res, 16: 45-58.

Suel, G. M., J. Garcia-Ojalvo, L. M. Liberman, and M. B. Elowitz. 2006. An excitable gene regulatory circuit induces transient cellular differentiation, Nature, 440: 545-50.

Teuscher, A. C., and C. Y. Ewald. 2018. Overcoming Autofluorescence to Assess GFP Expression During Normal Physiology and Aging in *Caenorhabditis elegans*, Bio Protoc, 8.

Topalidou, I., and M. Chalfie. 2011. Shared gene expression in distinct neurons expressing common selector genes, Proc Natl Acad Sci U S A, 108: 19258-63.

Tursun, B., T. Patel, P. Kratsios, and O. Hobert. 2011. Direct conversion of *C. elegans* germ cells into

specific neuron types, Science, 331: 304-8.
Walczak, A. M., J. N. Onuchic, and P. G. Wolynes. 2005. Absolute rate theories of epigenetic stability, Proc Natl Acad Sci U S A, 102: 18926-31.
Warren, P. B., and P. R. ten Wolde. 2005. Chemical models of genetic toggle switches, J Phys Chem B, 109: 6812-23.
Wicks, S. R., C. J. de Vries, H. G. van Luenen, and R. H. Plasterk. 2000. CHE-3, a cytosolic dynein heavy chain, is required for sensory cilia structure and function in *Caenorhabditis elegans*, Dev Biol, 221: 295-307.
Zhang, L., J. D. Ward, Z. Cheng, and A. F. Dernburg. 2015. The auxin-inducible degradation (AID) system enables versatile conditional protein depletion in *C. elegans*, Development, 142: 4374-84.

SUPPLEMENTARY FIGURES

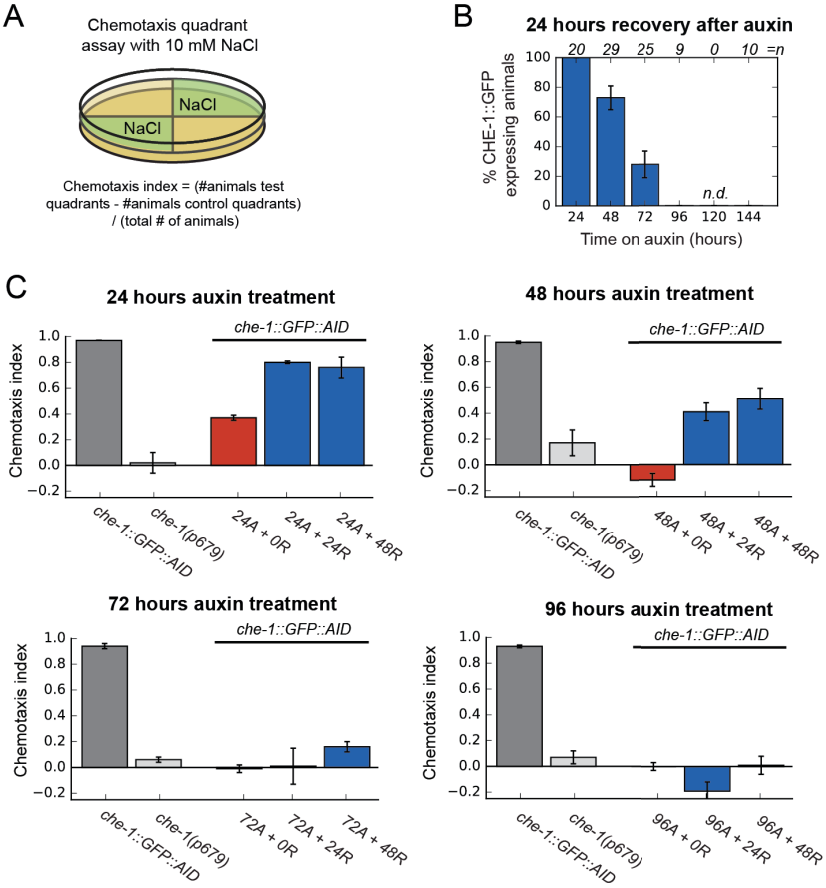

Figure S1. CHE-1 depletion leads to loss of ASE cell fate. (A) Schematic of quadrant chemotaxis assay and chemotaxis index (CI) calculation. **(B)** Percentage of animals that recovered CHE-1::GFP expression after auxin treatment of increasing length with a recovery period of 24 hours. **(C)** Chemotaxis index for wild-type, *che-1(p679)* and *che-1::GFP::AID* animals exposed to auxin for 24-96 hours after a recovery period of 0, 24 or 48 hours.

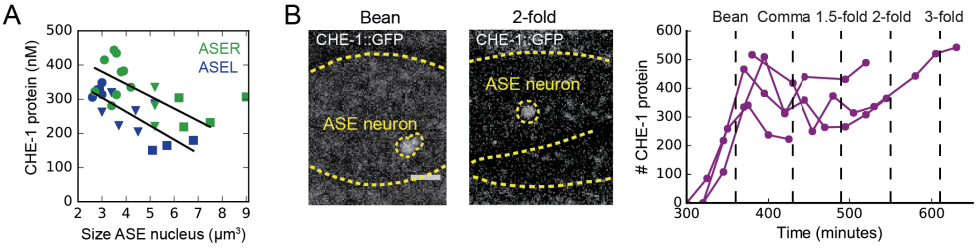

Figure S2. CHE-1 copy numbers in larvae and embryos. (A) CHE-1 protein concentration in ASER (green) and ASEL (blue) at different stages of post-embryonic development (L1/L2: circles, L3/L4: triangle, young adult: squares). CHE-1 protein concentration decreases with the age of the animals. **(B)** Images of *che-1::GFP* embryos for quantification of CHE-1::GFP in ASE neurons with confocal microscopy (left). Number of CHE-1 protein molecules over time in embryos, starting at the bean stage until twitching started (at 22 °C) (right). Embryos showed similar levels of CHE-1 protein as the L1 larvae.

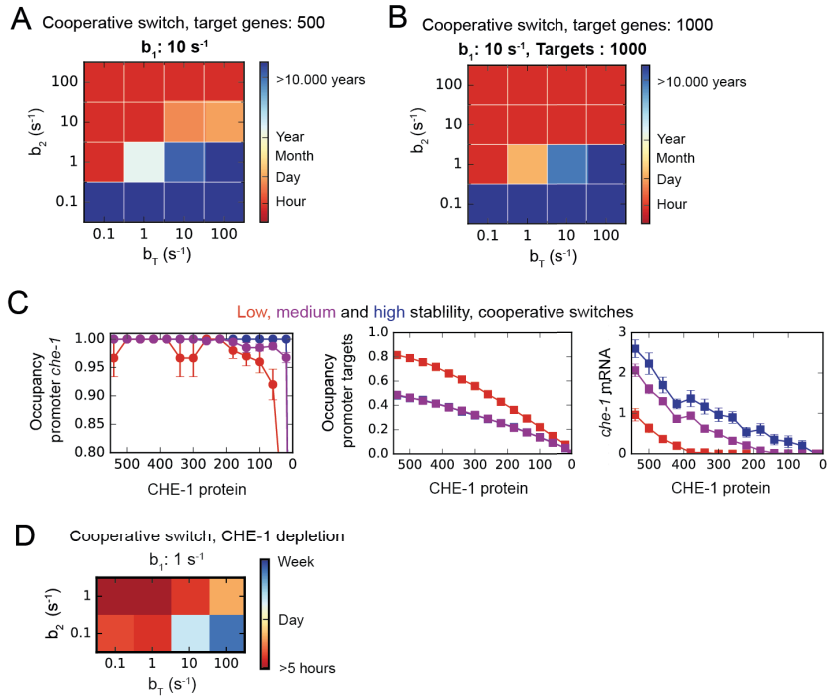

Figure S3. Dependence of ON state stability on number of targets and cooperativity. (A,B) Average ON state lifetimes calculated using Forward Flux Sampling (FFS) as function of the dissociation rates of CHE-1 from its own promoter (b_2,b_1) and target genes (b_T) promoters, for the cooperative model with O_T^* = 500 (A) or 1000 (B) CHE-1 targets. ON state lifetimes are lower for 1000 targets, but long lifetimes of many years are still found. b_1=10 sec^{-1} and b_1,b_T varied between 0.1 – 100 sec^{-1}. **(C)** Average CHE-1 occupancy of the promoter of *che-1* (left) and other target genes (middle), and average *che-1* mRNA level (right) during spontaneous transitions from the ON to the OFF state, as sampled by FFS, for the cooperative model. Shown are transition paths for parameters with low (red, b_2 ="100 s^{-1},b_T=10 s^{-1}.), medium (magenta, b_2 = 10 s^{-1}, b_1 = 100 s^{-1}),, and high (blue, b_2 = 1 s^{-1}, b_1 = 100 s^{-1}) stability of the ON state, with b_1 = 10 s^{-1}. **(D)** Average ON state lifetimes calculated using Forward Flux Sampling (FFS) of the cooperative model during depletion of CHE-1 protein, as function of the dissociation rates of CHE-1 from its own promoter (b_2) and its target genes (b_T), where b_1 = 10 sec^{-1}.

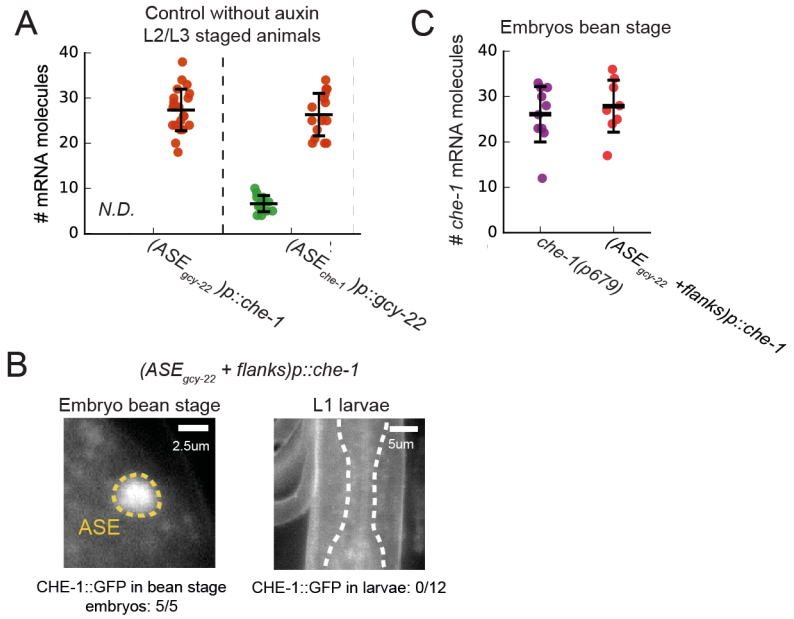

Figure S4. Controls for promoter region mutants. (A) Quantification of *gcy-22* (red) and *che-1* (green) mRNA levels in *(ASE$_{gcy-22}$)p::che-1* and *(ASE$_{che-1}$)p::gcy-22* L2/L3 animals without auxin revealed wild type mRNA levels for both genes. **(B)** CHE-1::GFP expression in *(ASE$_{gcy-22}$ + flanks)p::che-1* bean stage embryos and L1 larvae. Embryos showed CHE-1::GFP expression (5/5 animals), whereas L1 larvae no longer expressed CHE-1::GFP (0/12 animals). **(C)** *(ASE$_{gcy-22}$ + flanks)p::che-1* embryos showed similar levels of *che-1* mRNA during the bean stage as the *che-1(p679)* mutant.

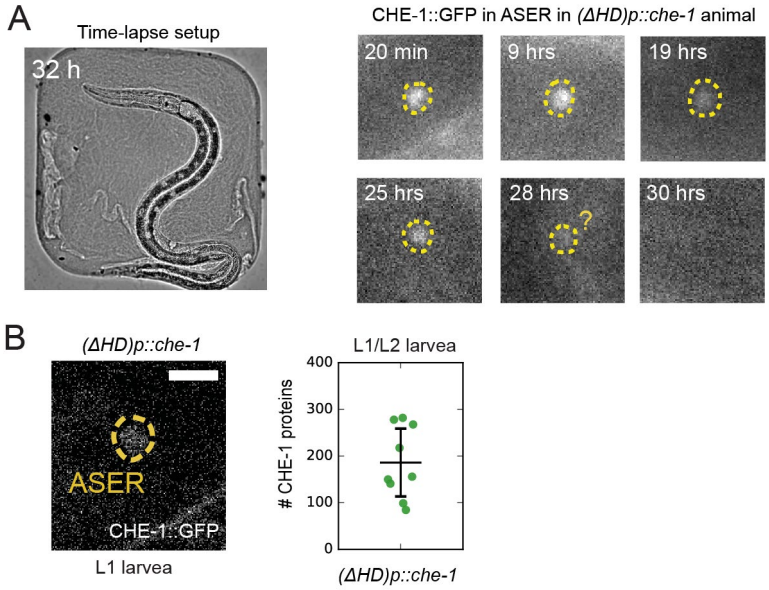

Figure S5. Time lapse imaging and quantification of CHE-1::GFP in *(ΔHD)p::che-1* animals. (A) Long-term time-lapse microscopy of a single *(ΔHD)p::che-1* animal, using microchambers to constrain larvae to the field of view (left). CHE-1::GFP expression in ASER disappeared rapidly in the L3 larval stage, 30 hours after hatching (right). **(B)** Image of CHE-1::GFP in *(ΔHD)p::che-1* L1 larva (left). Quantification of CHE-1::GFP protein in *(ΔHD)p::che-1* L1/L2 staged animals (right).